ABSTRACT

Title of Document: DESIGN AND IMPLEMENTATION OF THE FLAMING COMBUSTION CALORIMETER

Xi Ding, Master of Science, 2013

Directed By: Professor, Stanislav I. Stoliarov, Department of Fire Protection Engineering

Brominated flame-retardants (BFRs) were widely used for being high cost effective. However, due to the environmental concerns of BFRs, new flame-retardants with similar flame inhibition mechanism (gas phase combustion inhibition) need to be developed and tested for fire resistance. The current method for laboratory testing of fire resistance is on bench-scale Cone Calorimeter. This test requires relatively large samples and is extremely expensive for developing new materials. An innovative instrument called the Flaming Combustion Calorimeter (FCC) was designed, built and implemented to measure the heat release rate of flaming combustion of milligram-scale sample and the test result showed the FCC is able to detect the gas-phase combustion inhibition mechanism of bromine with good sensibility and repeatability.

DESIGN AND IMPLEMENTATION OF THE FLAMING COMBUSTION CALORIMETER

By

Xi Ding

Thesis submitted to the Faculty of the Graduate School of the
University of Maryland, College Park, in partial fulfillment
of the requirements for the degree of
Master of Science
2013

Advisory Committee:
Professor Stanislav Stoliarov, Chair
Professor James Quintiere
Professor Michael Gollner

Acknowledgements

First of all, I am heartily thankful to my advisor, Dr. Stanislav Stoliarov for his patience and guidance through every step of this project. The process of developing a new apparatus is full of trials and errors. At first, when facing a difficult problem, I got panic and just tried to fix it without knowing what the right scientific approach was. Dr. Stoliarov would talk me through the problem and help me identify the cause as well as suggest several scientific solutions to address the issue. His extremely broad knowledge and experience was the driving force behind the development of this project.

I would like to thank Fernando Raffan whom I collaborated with on this project. In addition to performing experiments with me and guiding me in the laboratory, he designed the gas analyzing system for the flaming combustion calorimeter, developed the Labview program for acquiring data as well as the Matlab program for processing data. Without his collaboration on this project, I would not be able to present the flaming combustion calorimeter as a fully functioning apparatus and the results would not be as impressive as those presented here.

I would like to thank all my group mates. They are all interesting, knowledgeable and hardworking individuals who helped me a lot during my stay here and made the office environment fun and positive. I would like to thank Ms. Olga Zeller for her

huge help in the laboratory, Ms. Mary L. Holt for ordering all the par t s for building the Micro-scale combustion calorimeter and the flaming combustion calorimeter.
I would like to thank the Federal Aviation Administration for providing the funding for this project, help with equipment and material samples from BASF and assistance from Dr. Richard Walters, Dr. Richard Lyon and Dr. Roland Kraemer.

My special thanks go to my family in China for their love and support. Words cannot describe my love for them and I could never thank them enough.

Table of Contents

List of Tables

List of Figures

Chapter 1: Introduction

1.1 General introduction

Polymer materials have been widely used across the world. Since many polymers are flammable in its pure form, they are typically blended with flame-retardants to increase the fire resistance； brominated flame-retardants (BFRs) have been the most used flame retardants because they are both effective and economical. However, due to the environmental concerns that BFRs tends to persistent in the environment and accumulate in human tissues, large chemical companies have been developing new materials to replace the BFRs; the flammability of those newly developed materials needs to be tested. One of the standard polymer material flammability testing method that performs heat release tests on the Cone Calorimeter requires polymer samples of approximately 100 g, which is extremely costly to conduct on new materials with flame-retardants. Thus, a milligram-scale screening tool is desired to test the heat release rate of flaming combustion of polymer samples and study the gas phase activity of small samples.

In this thesis, the mechanism of bromine as a combustion inhibitor is presented; bench scale flaming combustion heat release rate testing apparatus the cone calorimeter (CC) as well as milligram scale non-flaming combustion heat release rate testing apparatus the micro-scale combustion calorimeter (MCC) are introduced. The principle of oxygen consumption technique to measure the heat release rate that is

utilized in the CC, MCC and our apparatus is discussed. The development of our apparatus, the flaming combustion calorimeter (FCC) is introduced in detail; the test results of CC, MCC and CC for brominated flame retardants are presented and discussed.

1.2 Flame Retardants

1.2.1 Background

Natural and synthetic polymer materials have been widely used across the world and are becoming ubiquitous with their advantages in low density, customizable mechanical properties, easy processablity, etc. However, many polymer materials are inherently flammable in the pure form. In order to use these materials in certain commercial areas (buildings, vehicles, electronic appliances, etc…), flame retardant (FR) additives are typically blended with polymers to improve the fire resistance for many commercial applications. The major developments of flame retardants can be represented by the following: [1]

Chlorinated paraffin, antimony oxide;

Chlorine containing unsaturated poly(ester)s;

Filler-like retardants;

Oxygen index method of evaluating relative polymer flammability;

Intumescent flame retardant systems;

Inherently flame retardant polymers.

The combustion process is made up of four major steps in general: ignition, pyrolysis, combustion and feedback. In the presence of a source of sufficient heat, polymers will decompose and release flammable volatiles, which mix with air, and react in several rapid chain reactions to release energy in the forms of heat and light. [2] All flame retardants act either in the gas phase or the condensed phase through a chemical and/or physical mechanism to interfere with the combustion process during the heating, pyrolysis, ignition or flame spread. For example, filler-like retardants mainly act to dilute the polymer and reduce the concentration of pyrolysis gases. [3]There are also hydrated fillers that release non- flammable gases upon heating, or decompose endothermically to cool the pyrolysis zone. Phosphorus can promote char formation in the condensed phase to suppress the emission of flammable volatiles and shield the heat feedback from the flame to the pyrolysis surface. Phosphorous can also act in the gas phase similar to halogens and antimony, which interfere with the exothermic process of combustion. Another major agent is the intumescent flame retardant. In this method, materials swell when exposed to fire or heat to form a porous foamed mass, usually carbonaceous, that acts as a barrier to heat, oxygen and pyrolysis products. The relative comprehensive mechanisms via which the flame retardants work is introduced in the next section.

1.2.2 Modes of actions of flame retardants

Condensed phase

1. Physical mode:

There are several ways for the combustion process to be retarded by physical action in the condensed phase:

(1) Formation of a protective layer

Being heated, the flame retardant can form a protective layer with low thermal conductivity at the surface of the material. By shielding the heat feedback from the flame, the degradation rate of the polymer is reduced and the rates at which the gas-phase pyrolysis products enter the flame. [3]

(2) Cooling

Some additives, for example, ATH (aluminium trihydroxide), can degrade endothermally, which cools down the surface to a temperature below that required to sustain the combustion process. [4]

(3) Dilution

The incorporation of inert substances dilute the fuel in the solid phase so that there is a lower fraction of combustible fuel, which, in some case, can prevent ignition by ensuring the lower ignition limit of the gas mixture is not exceeded. [5]

2. Chemical mode:

Flame retardants can cause a layer of carbon (charring), a ceramic- like structure and/or a glass to be formed on the polymer's surface to slow down the surface pyrolysis rate. [4]

Gas phase

1. Physical mode:

The physical effects of having flame retardant in the gas-phase combustion zone are: dilution (adding dilutes to air decreases the oxygen concentration), heat capacity energy sink (removal of combustion energy) and changes with bath gas thermal conductivity. [4] The primary mode of physical suppression is energy removal by heat capacity effects. Indritz & Sheinson determined that heat capacity energy sink would account for over 70% of the physical suppression effect of agents CF4 and SF6 by making numerical flammability calculations on premixed hydrogen-air flames. [5] The effect of energy abstraction is important because it would decrease the flame temperature. When the flame temperature falls below approximately 1600 K, a hydrocarbon flame cannot self-sustain because the concentration of radicals decreases below a critical value required to propagate the thermal explosion required for combustion. [4] Also, there would be less energy feedback to the material surface for the pyrolysis of flammable volatiles.

As pointed out by R. Sheinson, et al, suppression effects due to dilution are present but small as a result of the large concentration of nitrogen already in the air. [4] By testing and comparing the amount of fire suppressants needed in the air mixture to extinguish a heptane diffusion flame, R. Sheinson et al were able to determine that other than helium, other agents have a small fraction of thermal conductivity effectiveness. As for helium, 20% of its effect is due to increased energy transfer via thermal conductivity.

2. Chemical mode:

As Warnatz [6] and Dixon-Lewis [7] have proposed, the dominant reactions in hydrocarbon oxidation flames are those for chain-branching

$$H + O_2 = OH + O \quad [1]$$

And the process that converts CO to CO_2

$$OH + CO = CO_2 + H \quad [2]$$

In flames, the hydro-carbon is attacked by the O, H and OH radicals that are produced in the course of the above reactions and keep decomposing to smaller molecules until oxidized. [8] Chain-branching steps increase the concentration of radicals and the production of CO_2 results in most of the heat that is produced during combustion. The rate constant of those reactions would control the burning velocity of the fuel. Reaction 1 is the main reaction that involves O_2 and the primary branching reaction for hydrocarbon air flames. [4] If its rate decreases, the radical pool of O, OH and H concentrations will also go down, thus the flame can no longer self-sustain itself and will extinguish eventually.

Chemical suppression requires direct intervention with flame reactions by creating reaction paths that compete with flame chemistry to reduce key radicals concentrations and key reaction rates. Take reaction 1 as an example, if the suppressant creates reactions that would act with hydrogen atom, the reaction rate of 1 would decrease as well as other propagation reactions.

There are three suppression actions for chemical mode: radical scavenging, i.e. removing reactive radicals by forming relatively unreactive radicals and molecules; participating in chain reactions that lead to radical recombination; and radical recombination enhanced by suppressant third bodies. [4]

1.2.3 Brominated flame retardants

Among all kinds of flame retardants, the brominated flame retardants are the most widely used additives because of their low cost and high performance efficiency. In fact, there are more than 75 types of commercial brominated flame retardants. [9] Brominated flame retardants belong to the family of halogenated flame retardants. The main mode of action of halogenated flame retardants is flame inhibition, i.e., the decrease in combustion efficiency as halogenated radicals trap reactive radicals during combustion to produce less reactive radicals. [8]

Halogenated molecules in the flame would create the following reactions with the reactive radicals like OH and H and convert them into more stable forms: [10]

$$RX \rightarrow R^{\cdot} + X^{\cdot} \ (X = Br \ or \ Cl) \quad [3]$$

$$X^{\cdot} + RH \rightarrow R^{\cdot} + HX \quad [4]$$

$$HX + H^{\cdot} \rightarrow H_2 + X^{\cdot} \quad [5]$$

$$HX + OH^{\cdot} \rightarrow H_2O + X^{\cdot} \quad [6]$$

RX is a hydrocarbon halide. Through equation 3 to 6, high energy $OH^{\cdot}$ and $H^{\cdot}$ radicals formed during combustion are removed (scavenged) by halogen radicals. Some combustible molecules are not fully oxidized, CO is produced and the heat release is significantly reduced. [10] And we can see from the above reactions, the Halogenated molecule can be recycled which makes them more effective.

Environmental concerns:

Despite the brominated flame retardants being effective in flame inhibition, they have been raising environmental concerns worldwide. Some brominated flame retardants have already been banned, such as poly-brominated biphenyls (PBBs) and tris (2, 3-dibromopropyl) phosphate (tris-BP). In the early 1970s, a poisoning incident in Michigan was attributed to the inadvertent mixing of PBB into animal feed, causing the death of livestock and leaving long-term impacts on the health of farm facilities in Michigan. The brominated flame retardant called “Tris- BP” which was originally used in clothing was removed from commerce because it was found to be mutagenic and nephrotoxic. [11]

The remaining brominated flame retardants in use will require basic toxicity testing, at minimum, before releasing to the market. However, recent reports by Alaee and Wenning [12] have shown that BFRs exist in the environment in locations far from where they are produced and/or used, and over time it has been observed that the concentration of BFRs has been increasing in both human-beings and animals.

1.3 Screening and Testing Instruments for Brominated Flame Retardant

1.3.1 Traditional flame retardant screening methods

The research and development of a new commercial polymeric material containing flame retardant typically goes through three stages. First, perform screening test and select flame retardant additives. Second, perform screening test to find the ratio of combination of flame retardant additives. Third, perform actual bench scale burning test of the material samples. [13]

Once the polymeric material with flame-retardants has been developed, it is required that the material pass one or several of the standard flame retardant testing methods depending on the target application of the material. Among those flame retardant testing methods, the following are the five main types [14]:

Ignitability tests (or UL94);

Flame spread tests;

Limited oxygen index (LOI);

Heat release tests (Cone calorimeter);

Smoke tests.

The UL94 test, Limited oxygen index test (LOI) and Cone calorimeter tests are discussed in detail.

Limited Oxygen Index: LOI

This test was first proposed in 1966 by Fenimore and Martin [15] and is used to indicate the relative flammability of materials. [16] It is standardized as the ASTM D 2863 test in the U.S. and ISO 4589 internationally.

According to ISO 4589, the LOI is measured on 80 × 10 × 4 mm^3 specimens placed vertically at the center of a glass chimney as shown in Fig. 1. The sample is burned within a controlled atmosphere with the mixture of gases flowing upstream through the chimney. After igniting the top of the sample like a candle, the O_2/N_2 ratio of the mixture is controlled to find the lowest oxygen concentration which just supports sustained burning. The criticality criterion is typically expressed as a minimum burning length: either specifying that the sample must burn for a certain length of time or that a specified length of material must be consumed.

The LOI is expressed as:

$$LOI = 100\frac{[O_2]}{[O_2] + [N_2]}$$

The higher is the LOI number is, the less combustible is the material. As air contains 21% oxygen, materials with an LOI below 21 are categorized to be “combustible” whereas those with an LOI above 21 are categorized as “self- extinguishing”. [17]

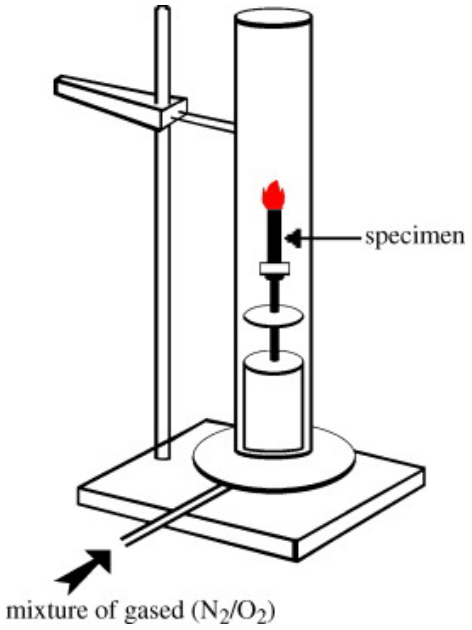

Fig.1. Experimental set-up for LOI measurement [17]

UL94V:

UL94 test includes a set of flammability tests approved by the “Underwriter’s Laboratories”: small and large flame vertical tests, horizontal tests for bulk and foamed materials, and a radiant panel flame-spread test. Among them, the UL94V test, which measures the ignitability and flame-spread characteristics of vertically-oriented bulk materials exposed to a small flame, is most widely used.

The schematic experimental set-up for the UL94V test is shown in Fig.2. Specimen size is 12.7mm by 127mm, with the thickness varying from 0.8mm to 3.2mm. The

test specimen is held on top of the burner with the distance between the bottom of the specimen and the top of the burner to be 10mm and remain unchanged throughout the test. The burner is controlled to produce a blue flame with a 20mm- high central cone and a heat release rate of 50W to ignite the sample. The flame is applied for 10s and removed. The after-flame time t_1 (the time required for the flame on the sample to extinguish) is recorded. After extinction, the flame is applied for another 10s and the after-flame time t_2 is recorded as well as after-glow time t_3. The specimen is then classified as V_0, V_1 or V_2 according to the criteria specified in the test standard. [17]

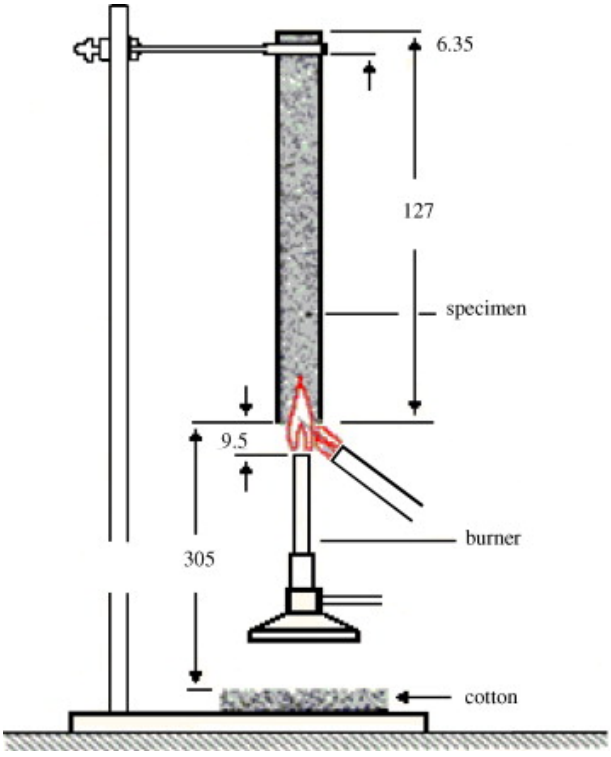

Fig.2. Experimental set-up for UL94V flammability test [17]

Cone calorimeter

The cone calorimeter test is one of the most effective bench-scale polymer fire behavior tests and is standardized as ASTM E 1354 in the U.S.. The principle of cone calorimetry is based on the O_2 depletion technique that will be discussed in section 1.4.1.

As shown in Fig. 3, the sample is heated by a conical radiant electrical heater, which simulates the burning surroundings in a room fire. The combustion gases produced pass through the heating cone and are captured by the exhaust system with a centrifugal fan and a hood. The gas flow rate, O2, CO and CO_2 concentrations as well as smoke density are measured in the exhaust hood. The cone calorimeter test also characterizes other properties like the time to ignition, time of combustion, mass loss rate and total smoke released.

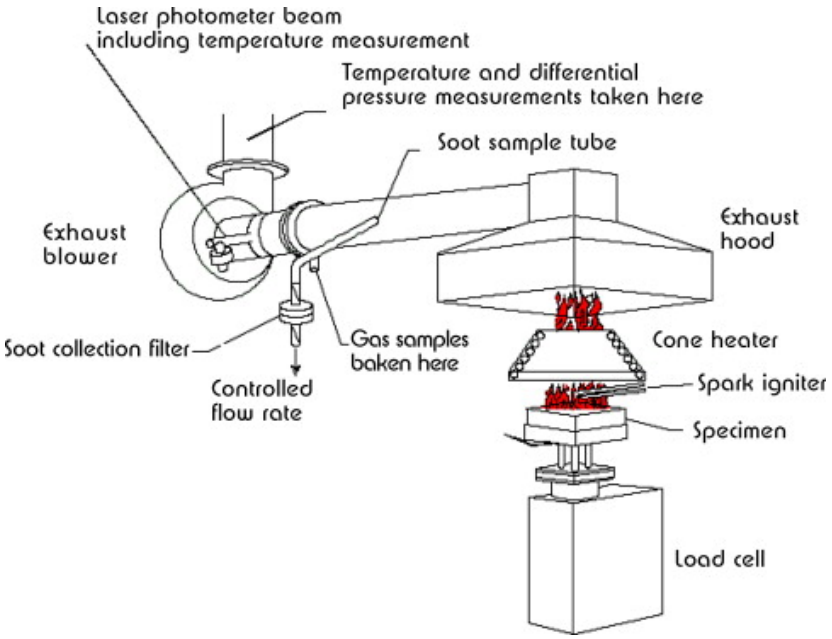

Fig.3. Experimental set-up for a cone calorimeter measurement [17]

1.3.2 Micro-scale combustion calorimeter (MCC)

The cone calorimeter test results for the brominated flame retardants showed that the gas-phase combustion efficiency decreases with an increase in the concentration of bromine, which is in accordance with the notion that bromine acts as gas phase combustion inhibitor. However, the cone calorimeter tests require replicate samples on the order of 100 grams each. To produce new polymeric materials with flame retardant for cone calorimeter tests would be very costly, thus, efforts have been made to develop laboratory instruments to measure the heat release rate of milligram-scale samples. [18]

The Federal Aviation Administration has developed an instrument named Micro-scale Combustion Calorimeter (MCC) that measures the heat of complete combustion of 1-5 milligram polymer samples through the implementation of analytical pyrolysis, combustion gas analysis, and flow calorimetry (i.e., pyrolysis-combustion flow calorimetry [PCFC]).

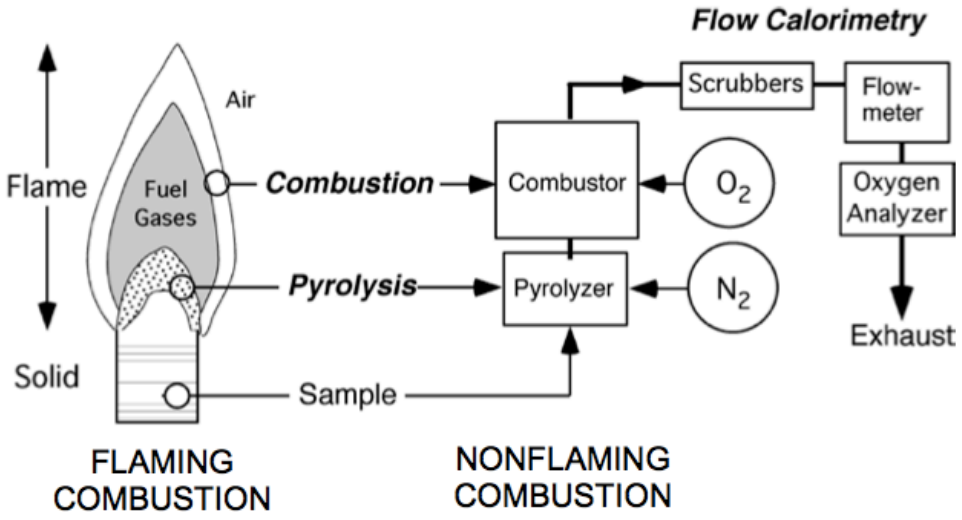

Fig.4. Illustration for pyrolysis-combustion flow calorimeter [19]

As shown in Fig. 4, the PCFC method incorporated in the MCC [18] decouples the condense phase pyrolysis process and the gas phase combustion process of an actual flaming combustion. Since in flaming combustion, the flame consumes all of the oxygen in the air above the specimen, the pyrolysis process is anaerobic. The pyrolyzer in the MCC simulates the pyrolysis process by pyrolyzing the sample at a constant heating rate in nitrogen flow. However, unlike flaming combustion, the gaseous products released in the pyrolyzer in the MCC are transported upward by the nitrogen flow to meet with impinging oxygen flow at 900 degree C for complete combustion. The heat release rate is measured by using the oxygen depletion technique. [20]

Bromine epoxies were tested in the MCC by Stanislav Stoliarov et al and the combustion efficiencies were calculated. [21] The calculated combustion efficiency

results were in conflict with the cone calorimeter test results in that the gas phase combustion efficiency increased slightly with the addition of bromine. Three main reasons can account for the discrepancy between the MCC and the cone calorimeter results. The first is the barrier effect, which becomes effective when an insulating layer could protect the underlying material from the heat source. The barrier effect does not affect the MCC results, but does affect the results of tests conducted in the cone calorimeter. [22] The second is that the combustion is complete in the MCC while the combustion efficiency in the cone calorimeter tests, even under well-ventilated conditions, is likely less than 1. Third, the temperature of the combustor in the MCC is 900℃, which is much lower than the flame temperature, which is around 1600℃. According to the observations summarized in reference [23], the role of bromine may change from an inhibitor of the gas-phase combustion to a promoter with decreasing temperature.

1.3.3. PFCC

Another method called the pyrolysis-flaming combustion calorimetry (PFCC) was developed by Stanislav Stoliarov et al [21] as the flaming modification of PCFC. The schematic diagram of PFCC method is shown in Fig 5.

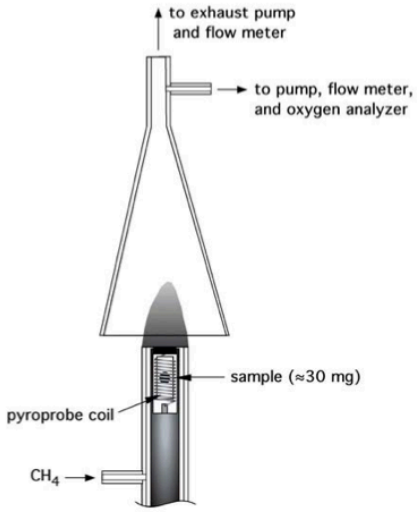

Fig. 5. The schematic diagram of PFCC[21]

In this method, a small sample of approximately 30mg was pyrolyzed at a constant heating rate. Pyrolysis products were swept by a methane flow(0.8 cm^3s^{-1}) to feed a laminar diffusion flame which was open to the atmosphere. The heat release rate was measured using oxygen depletion technique which will be introduced in detail in section 1.4.1.

The PFCC method was an attempt to directly measure the heat release rate of flaming combustion of a small scale sample that combined the methods of cone calorimetry and pyrolysis-combustion flow calorimetry. The PFCC is aimed at studying the gas phase combustion phenomena using a small scale sample and possibly screening the effectiveness of different flame retardants. However, the results of testing different brominated epoxies in the PFCC setup showed that the apparatus could not detect the gas phase combustion inhibition effect due to the presence of bromine in the sample.[21] Using methane as the purge gas to help create a diffusion flame could be the main reason of these results.

1.4 Oxygen Consumption Technique Background

1.4.1 General principle

As mentioned before, both cone calorimeter and MCC implement the principle of oxygen consumption technique to measure the heat release rate. The basic principle of oxygen consumption technique is introduced in this section.

In 1917, Thornton [24] discovered that for a large number of organic liquids and gases, an almost constant net amount of heat is released per unit mass of oxygen consumed for complete combustion. Later, Huggett [17] found this to also be true for most organic solids and obtained an average value for this constant of 13.1 kJ/g of O_2. Huggett's empirical observation implies that it is sufficient to measure the oxygen consumed in a combustion system in order to determine the heat released. This technique is now used extensively in many laboratories around the world in full-scale, bench-scale and small-scale fire tests instruments. The cone calorimeter, MCC and PFCC all use the oxygen consumption technique to obtain heat release rate data in the combustion process.

The basic requirement for this technique is that all of the combustion products are collected and removed through the exhaust duct. At a distance downstream sufficient for adequate mixing, both flow rate and composition of the gases are measured. [20] As a minimum, the O_2 concentration must be measured. However, the accuracy can

be improved by adding instrumentation for measuring the CO_2, CO and H_2O concentrations.

By the definition of oxygen consumption technique, the heat release rate $\dot{Q}$ can be described by the oxygen consumption rate $\dot{m}_{O_2}$ multiplied the constant 13.1 kJ/g.

$$\dot{Q} = 13.1 * \Delta\dot{m}_{O_2} \quad [7]$$

The oxygen consumption rate can be describe by the following equation,

$$\Delta\dot{m}_{O_2} = \dot{m}_{O_{2[IN]}} - \dot{m}_{O_{2[OUT]}} \quad [8]$$

Where $\dot{m}_{O_{2[IN]}}$ is the mass flow rate of O_2 into the system and $\dot{m}_{O_{2[OUT]}}$ is the mass flow rate of O_2 leaving the system.

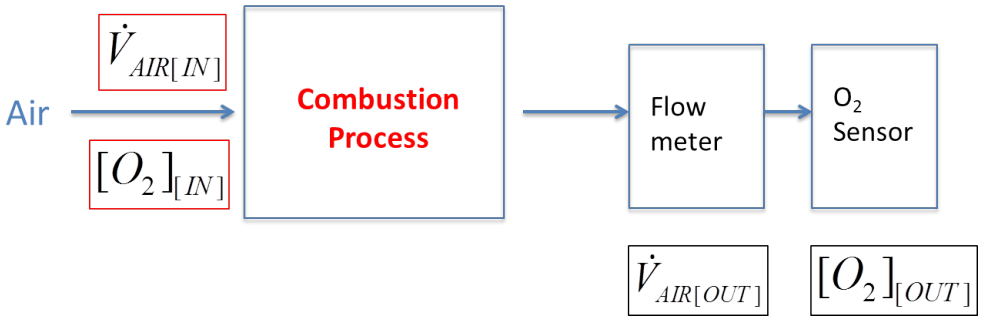

Fig. 6 Schematic of combustor using O_2 consumption technique

Further, the equation can be expressed as:

$$\Delta\dot{m}_{O_2} = \rho\dot{V}_{IN}[O_2]_{IN} - \rho\dot{V}_{OUT}[O_2]_{OUT} \quad [9]$$

Where ρ is the O_2 density at standard conditions, and $\dot{V}_{IN}$ and $\dot{V}_{OUT}$ are the volumetric flow rate at the same standard conditions flowing into and out of the system, $[O_2]_{IN}$ and $[O_2]_{OUT}$ are the oxygen concentrations in the inlet flow and the outlet flow as shown in Fig. 6. Usually in a combustor system that utilize the O_2 consumption

technique only a flow meter and an O_2 sensor are placed at the exhaust flow, thus, $\dot{V_{OUT}}$ and $[O_2]_{OUT}$ are measured directly while assumptions need to be made about $\dot{V_{IN}}$ and $[O_2]_{IN}$. Typically, there are two kinds of assumptions.

In the first assumption, $\dot{V_{IN}}$ is assumed as the baseline value in exhaust flow meter before test starts and stays constant throughout the test and $[O_2]_{IN}$ is assumed as the baseline value in oxygen sensor before the test starts and stays constant throughout the test as shown in Fig. 7.

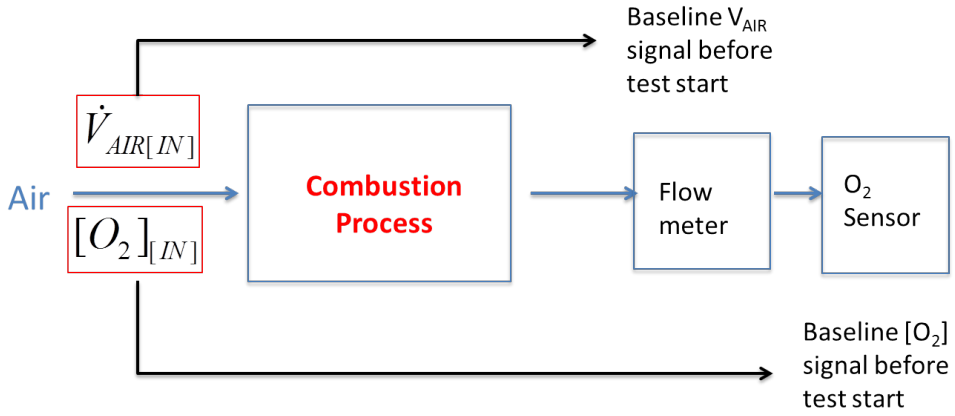

Fig.7. Assumption 1 about $\dot{V_{IN}}$ and $[O_2]_{IN}$

In the second assumption, $[O_2]_{IN}$ is still assumed as the baseline value in oxygen sensor before the test starts and stays constant throughout the test, however, $\dot{V_{IN}}$ is assumed to be the same as $\dot{V_{OUT}}$, which is the volumetric flow rate measured at the exhaust flow meter that change with time. Fig. 8 shows the schematic diagram of the second assumption. Thus, the following equation is used.

$$\Delta \dot{m}_{O_2} = \rho \dot{V_{OUT}} ([O_2]_{IN} - [O_2]_{OUT}) \quad [10]$$

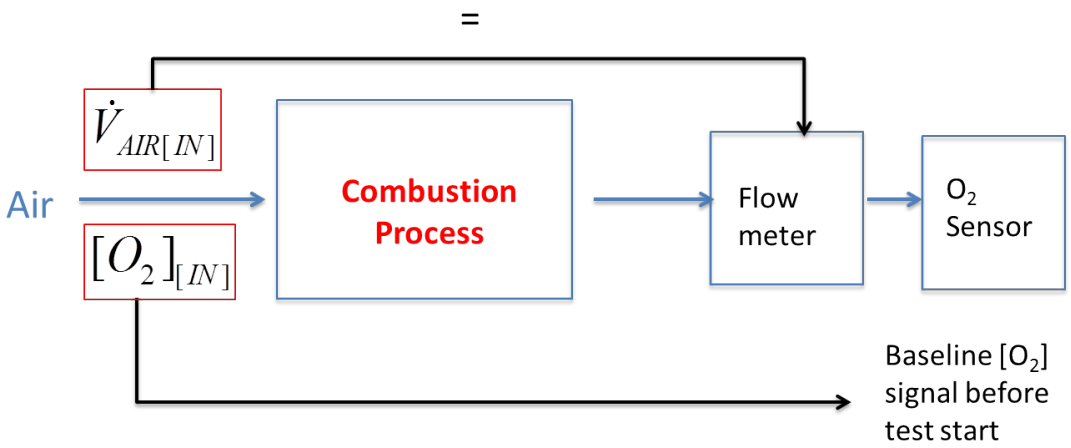

Fig.8. Assumption 2 about $\dot{V_{IN}}$ and $[O_2]_{IN}$

1.4.2 Application of oxygen depletion technique in cone calorimetry and MCC

For open system like cone and room fire test, it is not possible to measure the air flow rate into the system directly. The volume flow rate is measured downstream after the gases have undergone expansion due to chemical reactions. The oxygen sensor used in cone calorimeter is the paramagnetic oxygen sensor that based on the knowledge that oxygen has a relatively high magnetic susceptibility as compared to other gases such as nitrogen, helium, argon, etc. and displays a paramagnetic behavior. [21] The paramagnetic oxygen sensor is able to measure the oxygen level over the range of 0% to 25% within the accuracy of 50ppm.

For closed systems like MCC, the mass flow rate of the air into the system can be measured directly. Thus, equation 9 can be used to perform the oxygen consumption rate calculation although the software of MCC uses equation 10 to calculate the oxygen consumption rate. The oxygen sensor used in MCC is a R17-A micro-fuel cell from Teledyne Technology that converts chemical energy to electrical energy. The electrical output from the rate of this reaction is linear and directly proportional to the oxygen concentration. [18] The R17-A O_2 sensor can measure the oxygen level over the range of 0%-100% with the accuracy of $\pm$ 1%.

1.5 Objectives

The cone calorimetry tests are able to detect whether bromine acts as a gas-phase combustion inhibitor. However, the cone calorimetry tests require a sample size that is too costly for developing and testing new flame retardant compounds. Besides, the cone calorimetry tests cannot separate the effects on gas-phase combustion and the condensed-phase combustion. The MCC apparatus is capable of separating condensed-phase pyrolysis from gas-phase combustion for milligram-scale samples. However, the MCC cannot detect the effect of gas-phase combustion inhibition due to the presence of brominated flame retardants in the material. This is probably due to some mechanisms in the reactions of the brominated flame retardants being lost in the non-flaming pyrolysis and subsequent oxidation process in the MCC.

The objective of this study is to design and implement an apparatus that can study the gas-phase flaming combustion of milligram-scale materials in a well-controlled fashion and correlate the gas-phase combustion efficiency result with cone

calorimetry results. The condensed-phase and gas-phase combustion will be decoupled, both the inlet and outlet gas flow will be measured and the heat release in the gas-phase combustion will be measured via oxygen consumption technique. Furthermore, the system will be able to achieve both well-ventilated and under-ventilated conditions to study flaming combustion under those conditions.

Chapter 2: Development of the Flaming Combustion Calorimeter

2.1 General Guideline

The desired functions of the Flaming Combustion Calorimeter (FCC) included acquiring heat release rate via oxygen consumption technique to detect a sensible drop in combustion efficiency due to the addition of bromine to the test material, providing optical access to the flame so that the combustion time, flame height and flame structure could be observed; and serving as a research tool to study laminar diffusion flame under both well-ventilated and under-ventilated conditions.

In order to detect the gas phase combustion inhibition mechanism of bromine, as with the cone calorimeter, similar features to the cone calorimeter were implemented. As in the cone calorimeter, the FCC used oxygen consumption technique, created a diffusion flame and the airflow condition under which the combustion took place remained well-ventilated and semi-quiescent.

To provide optical access to the flame while keeping the system enclosed, a transparent quartz tube with low thermal expansion coefficient and low thermal conductivity coefficient was used for the combustion chamber. In order to use the FCC as a research tool to study well-ventilated and under-ventilated laminar diffusion flames, the airflow flow rate into the system was monitored across a wide range and the O_2 concentration in the inlet airflow was variable.

The Flaming Combustion Calorimeter was designed and implemented by Xi Ding and Fernando Raffan under the guidance of Dr. Stanislav Stoliarov in the University of Maryland based on the above guidelines. A schematic diagram of the FCC is shown in Fig. 9.

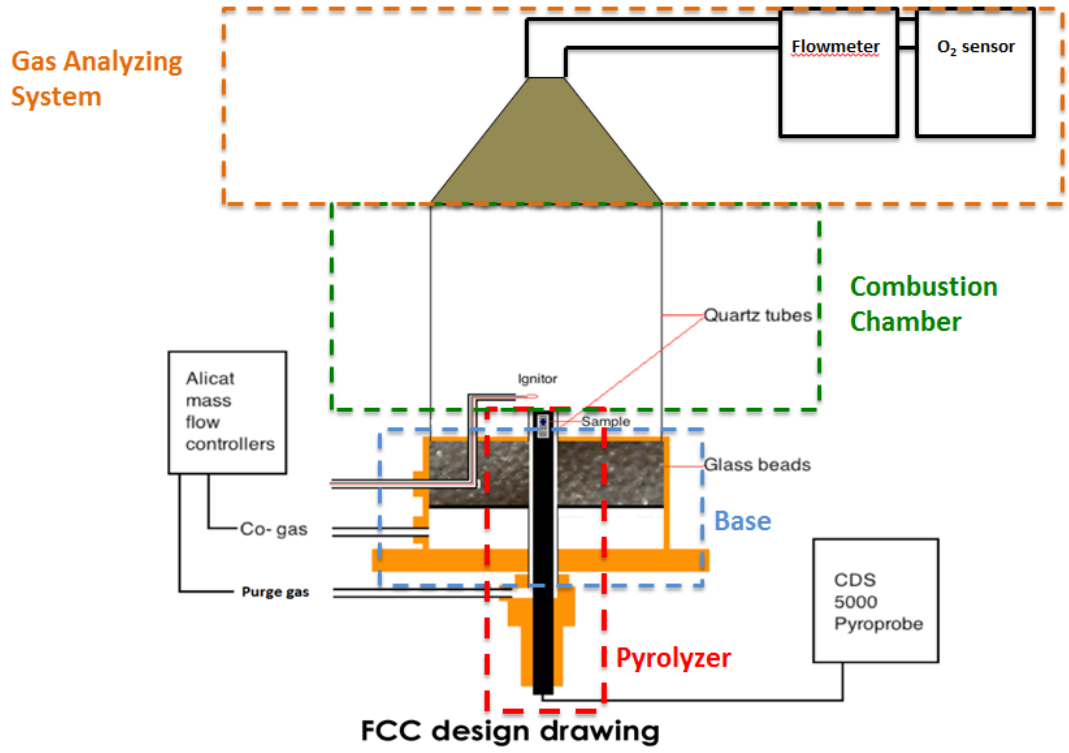

Fig.9.The schematic diagram of FCC

As shown in the schematic diagram, the FCC in essence consisted of four parts: the pyrolyzer, the base, the combustion chamber and the gas analyzing system. Those four parts will be discussed in detail in section 2.2. In the FCC, a sample of approximately 30mg was being heated in the pyrolyzer and the pyrolysis products were swept by the purge gas to meet with co-flow, which is co-gas in Fig. 9 for flaming combustion. The co-gas, which formed the combustion environment, could be air from the air bottle, or the mixture of o2 and n2 with controlled ratio so that the

flame performance under both low o2 concentration and high o2 concentration environments could be studied. The flow rates of co-gas and purge gas were controlled by mass flow controllers. The base served to get a homogenized, semi-quiescent co-flow and introduce igniter. The actual flaming combustion took place in the combustion chamber which was made of quartz tube that had extremely low thermal expansion coefficient and was transparent so that we could get the flame height, combustion time, time to ignition information. The combustion products were collected by the exhaust hood and volumetric flow rate and o2 concentration in the exhaust flow were measured to perform heat release rate calculation through o2 consumption technique.

2.2 Instrumentation of FCC

2.2.1 Pyrolyzer

The pyrolyzer consisted of a heating element and a quartz tube. The heating element was a model 5000 pyro-probe from CDS Analytical Company as shown in Fig.10.

Fig.10. CDS 5000 Pyro-probe [24]

There was a platinum filament in the pyro-probe, whose temperature profile could be programmed to have up to 8 steps and the heating rate could vary from 0.01℃/sec to 999℃/sec. The maximum temperature that the platinum filament could achieve was 1400℃. In this case, the temperature profile of the platinum filament was programed in three steps: initial, ramp and final. At the initial stage, the filament was programmed to hold at 30℃ for 5 s. At the ramp stage, the filament was programmed to heat up at a given heating rate and when it reached to the final stage, the temperature of the filament was programmed to hold at 1200℃ for 2 min.

As shown in Fig.11, the pyro-probe was surrounded by a quartz tube. The diameter of the pyro-probe was 0.5 inch, and the inner diameter of the quartz tube was 13mm. This was slightly larger than the diameter of the pyro-probe such that the purge gas could enter through the gap between them. The outer diameter of the quartz tube was 5/8 inch such that the quartz tube would fit into a 5/8 Swagelok fitting for sealing.

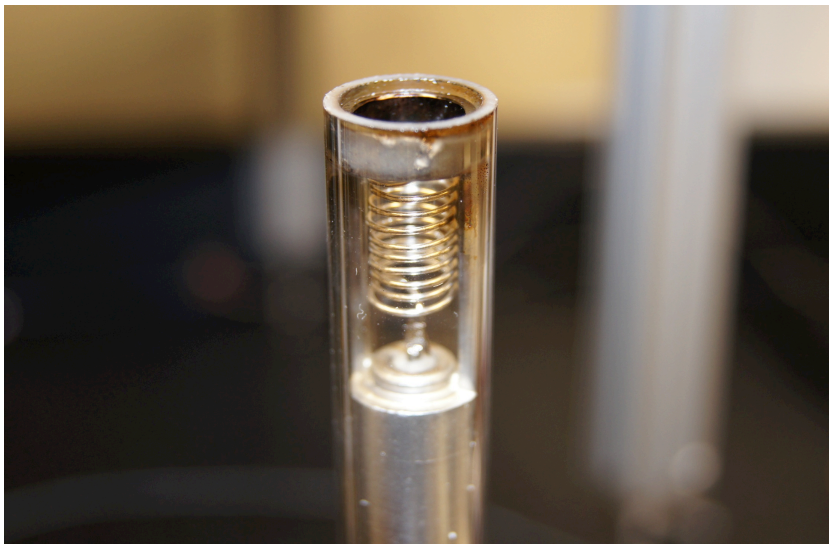

Fig.11.The pyro-probe with quartz tube

A Swagelok factory special fitting (B-1010-3-8-6), a brass tee of 3/8 inch, ½ inch and 5/8 inch threaded connections was used to connect the pyro-probe, quartz tube and the purge gas tube as shown in Fig. 12. The purge gas could be either N_2 or a gas fuel with its rate controlled by a mass flow controller. When pyrolyzing solid polymer samples, N_2 was typically used as the purge gas to sweep the pyrolysis products up to meet with air while not interfering much with the combustion process. When studying the flame formed by gaseous fuels, a gas fuel such as methane or propane was used as the purge gas.

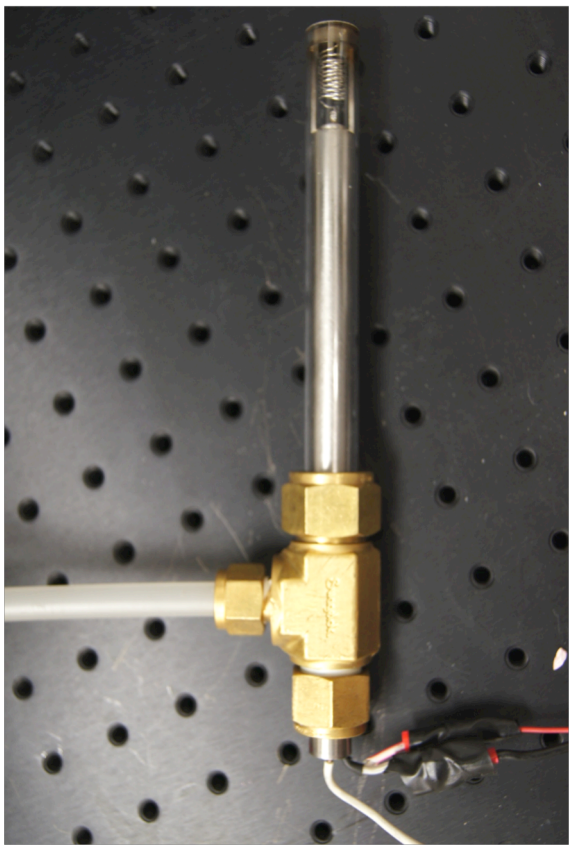

Fig.12.The pyrolyzer

2.2.2 Base

The base consisted of a brass cylinder with an outer diameter of 3.5 inch and a height of 1.9 inch together with a brass cuboid with the length and width of 5 inch and a height of 0.25 inch. The function of the base is to homogenize the co-flow, introduce the igniter as well as connect the pyrolyzer and the combustion chamber. The diameter of the base cylinder was chosen such that the co-flow would be semi-quiescent. The height of the base was chosen such that the filament of the pyro-probe could be above the base, thus visible.

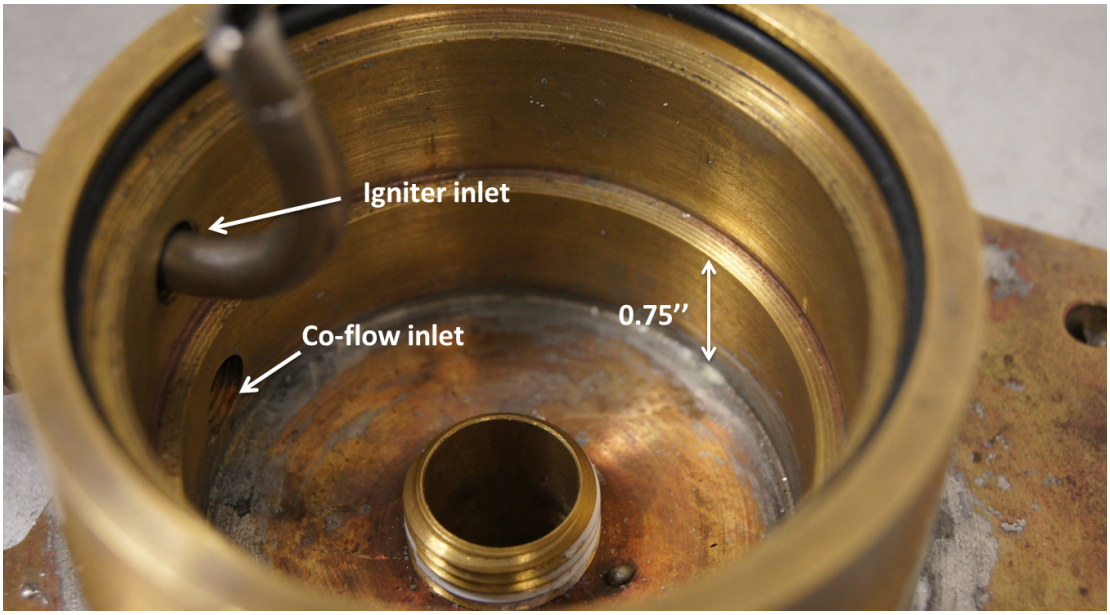

Fig.13.The inside of the brass base

As shown in Fig. 13, there were two holes along the wall of the base. The co-flow gas flowed through the hole near the bottom of the base. The other hole was used to insert the igniter. Swagelok fittings were used at these connections to prevent leakage. A circular perforated brass sheet rested on a circular lip 0.75 inch from the bottom of the

base. The perforated brass sheet had a hole in the center, allowing the pyro-probe to pass through. The space between the perforated brass sheet and the top of the base was filled with glass beads. Both the perforated sheet and the glass beads served to homogenize the co-flow. The burner had an O-ring grove at the top to connect the combustion chamber air-tightly. The combustion chamber would then sit on the circular edge 1.557 inch from the bottom of the burner as shown in Fig.14.

Fig.14.The assembly of the base and the pyrolyzer

2.2.3 Combustion Chamber

The combustion chamber was made up of a clear quartz tube with an inner diameter of 70mm, an outer diameter of 75mm, and a height of 5 inch. The inner diameter was chosen such that for the flow rates of interest, the actual linear velocity of the co-flow was slow to achieve semi-quiescent condition. The height was chosen to ensure

flame visibility. A clear quartz tube was chosen for the combustion chamber because of its extremely low thermal expansion coefficient, relatively low thermal conductivity and optical transparency. Half of the inner surface of the quartz tube parallel to its axis was painted with unreflective black paint to reduce refection of the flame in order that the flame height could be determined with relatively higher accuracy. This assembly is as shown in Fig.15. The igniter, which was made of 5 inch of 28 gauge NI80/CR20 wire was inserted through the base and enclosed in the combustor as shown in Fig. 15.

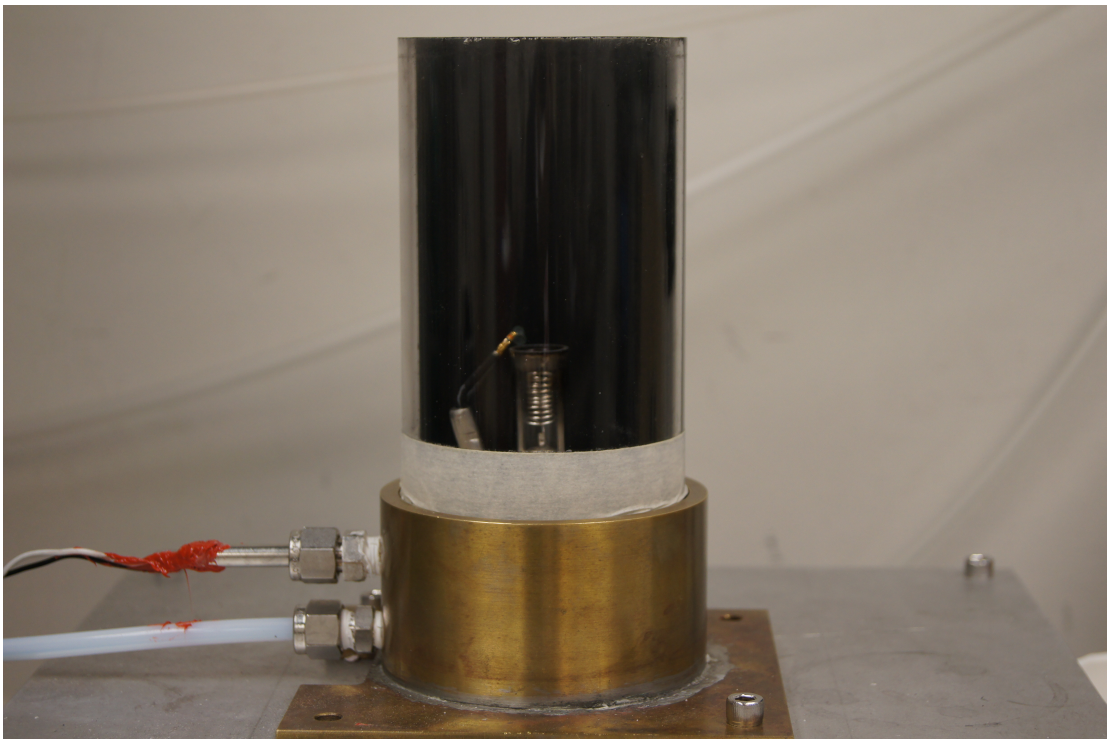

Fig.15.The assembly of base, pyrolyzer and combustion chamber

2.2.4 Gas Analyzing System

The gas analyzing system consisted of a hood, a soot filter, a tube filled with Drierite, a high accuracy flow meter and a micro-full cell oxygen sensor, as shown in Fig.16. The pressure gauge was used to monitor the pressure change in the sampling line; the soot filter was used to clean the flow as well as measure the soot yield as the soot filter was weighed before and after each test. The soot filters used were Whatman glass microfiber filters as shown in Fig. 17. The surface shown on the left that appears to be rougher faced the incoming flow. The oxygen sensor used in the FCC was a micro-fuel cell (Teledyne R17A). The oxygen sensor converts chemical energy to electrical energy. The electrical output from the rate of this reaction is linear and directly proportional to the oxygen concentration. [18] The Drierite was used to remove moisture so that the O_2 sensor would not be damaged.

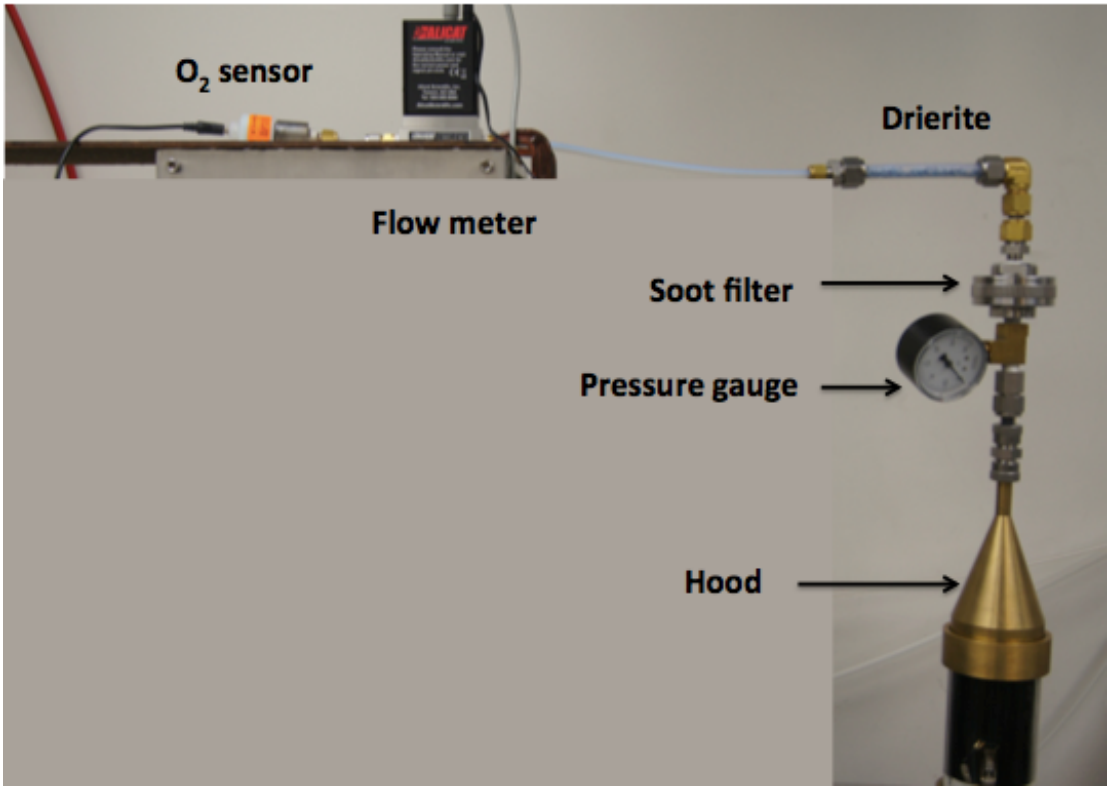

Fig.16.The gas analyzing system

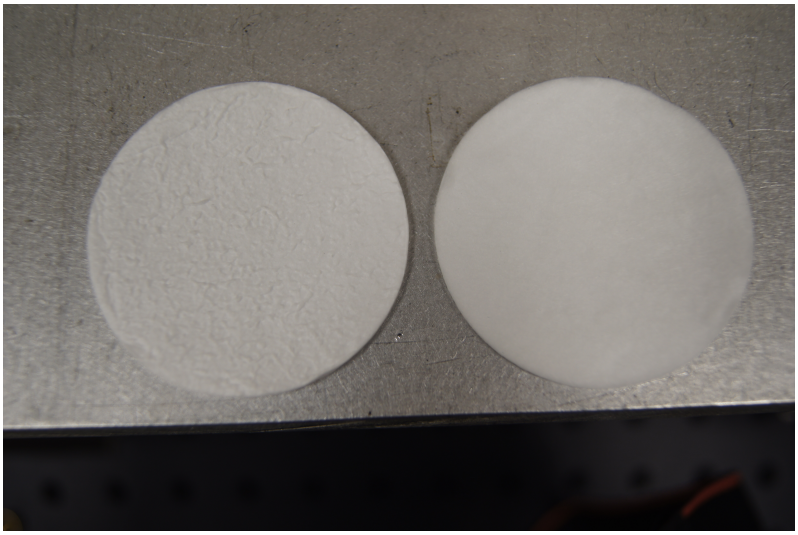
Fig.17.The two surfaces of the glass microfiber filter

2.2.5 Mass flow controllers

The co-flow was made up of oxygen and nitrogen flow with a ratio similar to air. The flow rates of oxygen and nitrogen gases were controlled separately by two mass flow controllers. The ranges of these mass flow controllers were carefully chosen to ensure accuracy. In order to make a reasonable estimation, the required mass flows of O_2 and N_2 for supporting the combustion of a 30mg (the estimated sample mass in FCC at this point) PMMA sample were estimated with the criterion that the O_2 concentration in the air during the combustion process would not drop below 20% of the original O_2 concentration.

The normalized mass loss rate of PMMA was provided by my colleague Jing Li through thermogravimetric analyses at the heating rate of 1 K/s: 3.48×10^{-3} s^{-1}. Thus the mass loss rate of a 30mg PMMA sample under the heating rate of 10 K/s (10 K/s was the estimated heating rate of FCC) was calculated to be 1.044×10^{-3} g/s. The chemical equation for PMMA combustion is:

$$(C_5H_8O_2)_n + 6nO_2 \rightarrow 5nCO_2 + 4nH_2O \qquad [11]$$

From the above equation, the O_2 consumption rate was calculated to be 6.264×10^{-5} mole/s. Because the O_2 consumption accounted for 20% of the whole O_2 supplied, the total O_2 flow rate was calculated to be 3.2×10^{-4} mole/s, and the total N_2 flow rate was 1.2×10^{-3} mole/s. By multiplying the molecular weight of O_2 and N_2, the mass flow rates were found to be 1.1×10^{-2} g/s for O_2 and 1.15 g/s for N_2. After dividing the mass flow rates by their densities at standard conditions and performing unit conversions, the O_2 and N_2 flow rates needed to meet the above criterion were

calculated to be 504 sccm (sccm: standard cubic centimeters per minute) and 1.8 slpm (slpm: standard liter per minute). To expand the flow range more than the calculated values could generate greater flexibility without sacrificing much accuracy, thus, 2 slpm as the range for O_2 and 5 slpm as the range for N_2 were determined for the co-flow mass controller.

2.3 Preliminary tests on FCC

2.3.1 Co-Flow Homogeneity test

Since there was only one inlet for the co-flow and the gas needed time to spread across the burner, the gas near the inlet would begin to travel upward sooner than the gas further away from the inlet. For this reason, a perforated brass sheet and glass beads were used to homogenize the flow. To test the homogeneity of the co-flow, the flow first passed through a bottle containing dry ice before entering the burner and the combustion chamber such that the flow path was visible. The result is shown in Fig.18 and suggests good homogeneity in the co-flow.

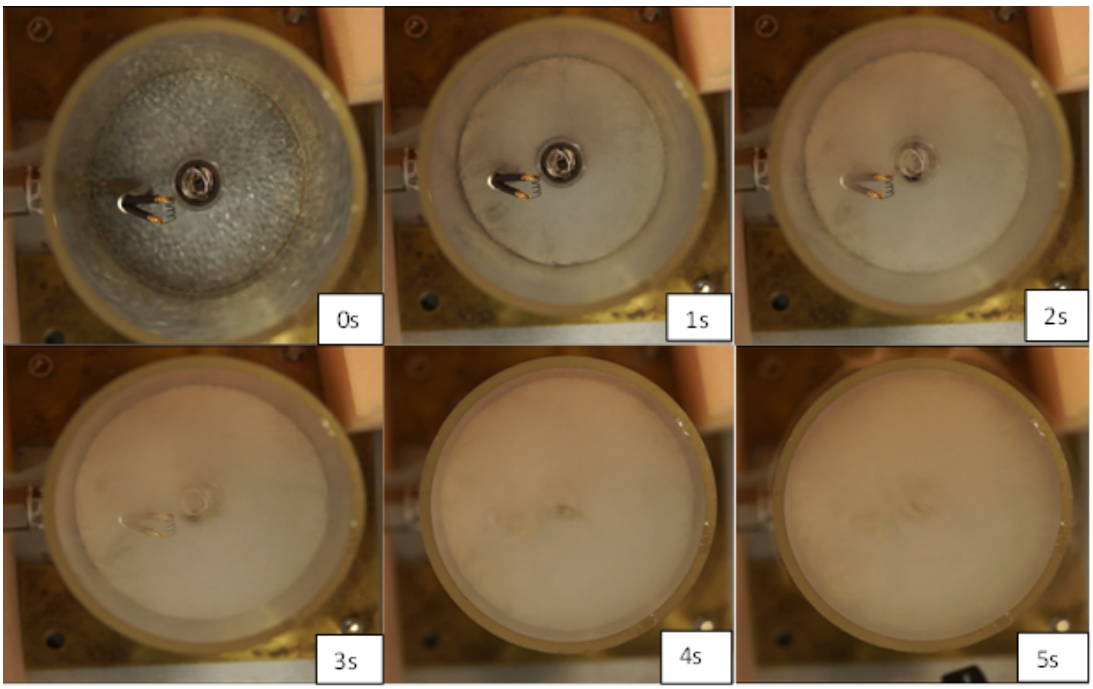

Fig.18.Co-flow homogeneity test: visualization of the flow path

2.3.2 Co-Flow Flow Rate Test

The impact of co-flow flow rate on the structure of the flame was also explored in the FCC. As shown in Fig. 16, a small blue flame was ignited and sustained with the purge gas being propane at the supplying rate of 15sccm. N_2 and O_2 were mixed in a 79% and 21% proportion by volume respectively in the co-flow and the co-flow flow rate was varied. Fig. 19 showed that the co-flow flow rate does have an impact on the flame performance.

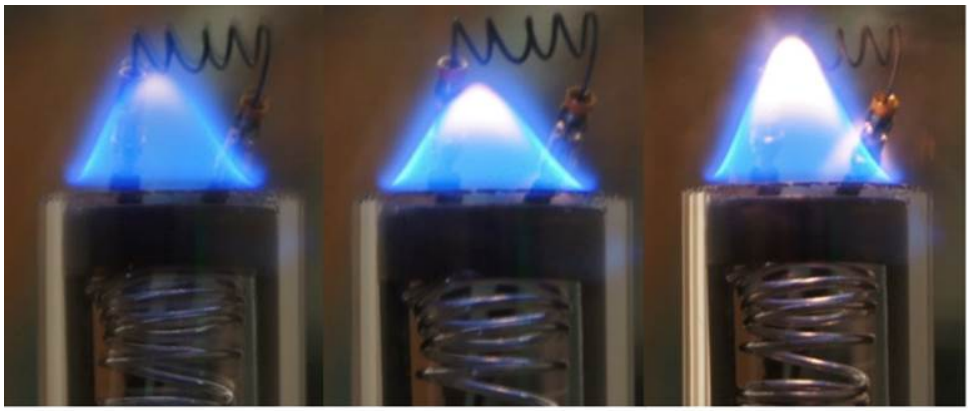

Fig.19.Co-flow flow rate test

At the co-flow flow rate of 0.5 slpm, which is the lowest possible flow rate that the mass flow controllers could deliver, the linear velocity of the co-flow was calculated to be 0.18×10^{-2} m/s. At the co-flow flow rate of 6.32 slpm, which is the highest possible flow rate that the mass flow controllers could deliver, the linear velocity of the co-flow was calculated to be 2.28×10^{-2}m/s. As Fig.19 shows, as the ventilation improved, the flame became more luminous and visible, suggesting the flame might become hotter. The propane flow rate was chosen close to the minimum that could generate a sustained diffusion flame and the test showed that this flame could be maintained over a wide range of co-flow flow rates, indicating the FCC would allow researchers to study flame under different ventilation conditions.

2.3.3. Combustion Chamber Oxygen Concentration Test

As shown in Fig. 20, a test was carried out to evaluate the impact of oxygen concentration of the co-flow on the flame structure. The purge gas was propane with its flow was set at 55sccm and ignited. The propane flow rate was chosen to establish

a flame of a size comparable to a polymer flame. The oxygen concentration in the co-flow was adjusted up and down while the total flow rate of the co-flow remained constant. The oxygen concentration in the left picture was 16%; it was the lowest oxygen concentration to maintain a propane flame in the FCC. The flame stretched allowing it to receive more oxygen for reaction. The bottom of the flame was almost transparent and the top yellow part was less bright, suggesting that little soot was produced. Despite that low oxygen concentration in the co-flow was indicative of incomplete combustion; soot exists at relatively high temperature. This observation that the flame was producing less soot at low O_2 concentration could be explained that the flame was not hot enough to produce soot abundantly. The picture on the right shows a flame with an oxygen concentration in the co-flow of 30%. This flame was shorter and much brighter than a flame in air. Since the O_2 gradient was larger in this flame, the overall diffusion rate of O_2 should go up. And it appeared that the diffusion of O_2 was faster and the combustion reaction went more vigorous in this case.

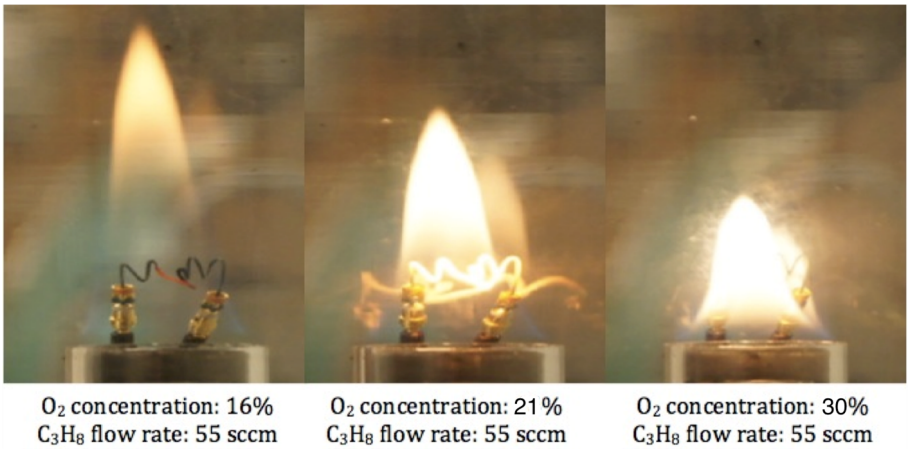

Fig.20.Combustion chamber Oxygen concentration test

Although tests in FCC were usually performed at O_2 concentration of 21% in the co-flow, this test showed that the FCC would allow a researcher to study flaming combustion of polymers under various O_2 concentrations.

2.3.4. Choosing heating rate for sold material test

The appropriate heating rate that could burn most of the fuel for the FCC was determined via combustion time versus heating rate tests since the oxygen consumption analysis system had not been developed yet. PMMA was chosen to be the sample material because in its pure form, it is a well characterized polymer that burns relatively cleanly with no char, very little soot and does not condense. The combustion times of a series of 30mg polymethylmethacrylate (PMMA) samples at various heating rates were recorded and plotted against heating rates as shown in Fig. 21. The combustion time was defined to be the time between ignition and extinguishment of the flame. The purge gas of N_2 was maintained at a flow rate of 10sccm. At lower heating rates, 1K/s and 2K/s, the flames were small and blue with flickering features, but persisted for relatively long periods of time, approximately 1 min. As the heating rate increased, the flame became taller and more luminous, but the combustion time decreased. Intuitively, the heating rate in the middle that generated a steady flame with adequate combustion time was desired. Yet a more scientific method needed to be employed to determine the right heating rate.

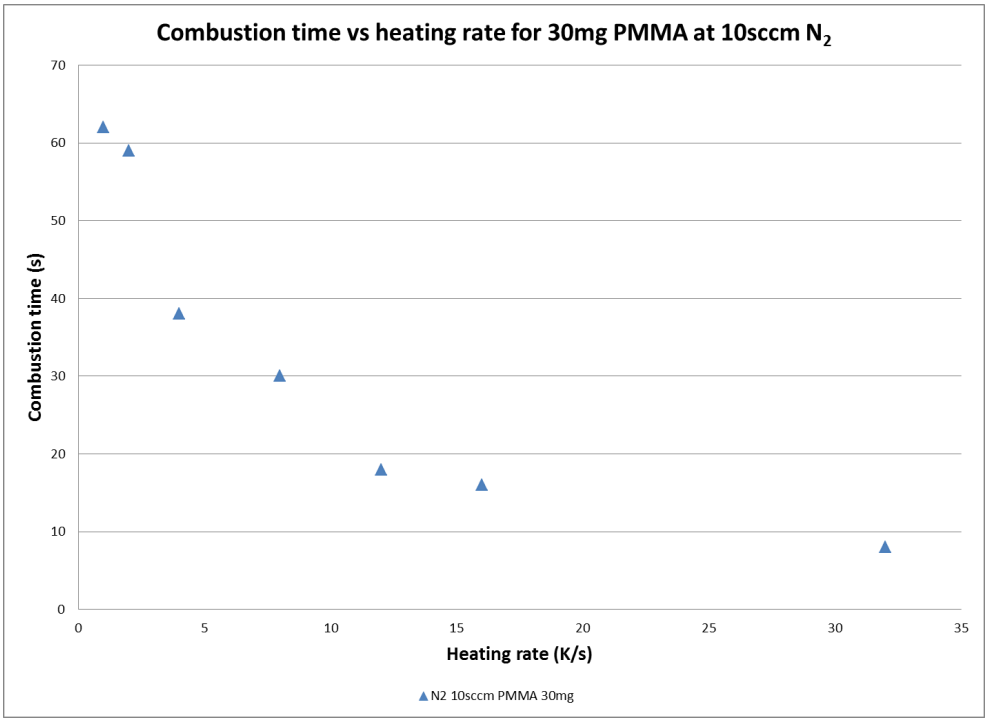

Fig.21.Combustion time versus heating rate tests for PMMA

For the first-order pyrolysis of a polymer with volatile mass of m and non-combustible mass of m_c, we have:

$$-\frac{dm}{dt} = k(m - m_c) \qquad [12]$$

With k as rate constant satisfies the Arrhenius equation:

$$k = Aexp\left(-\frac{E_a}{RT}\right) \qquad [13]$$

Where,

A is the frequency factor describes the number of potential elementary reactions per unit time, E_a is the activation energy that describes the energy barrier that must be exceeded in order for a reaction to occur,

R is the universal gas constant,

T is the reaction temperature.

Equation 12 was solved numerically in Matlab (m_c =0, A=10^{12} s^{-1}, E_a=160 kJ/mol was used for PMMA) [25] and the normalized mass loss rate curves versus time were plotted for heating rate at 2K/s, 6K/s, 10K/s ans 14 K/s as shown in Fig. 22. The integrals of the four curves should be the same and all equal to 1. Assuming that 90% of the total fuel mass was burned in flaming combustion at the four heating rates; the combustion time could be acquired, which is plotted in Fig. 23.

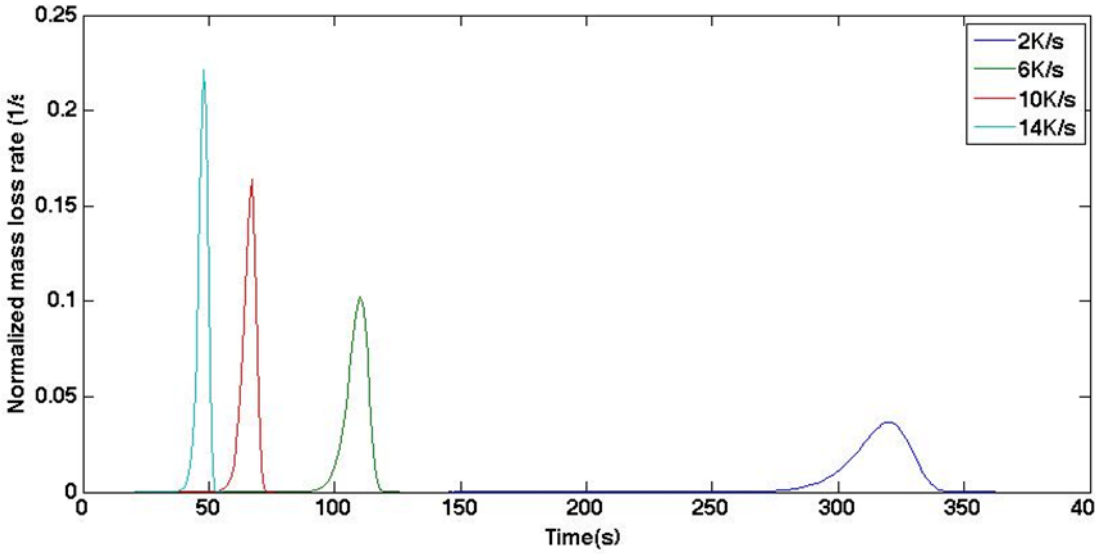

Fig.22.Numeric solution of normalized mass loss rate plots

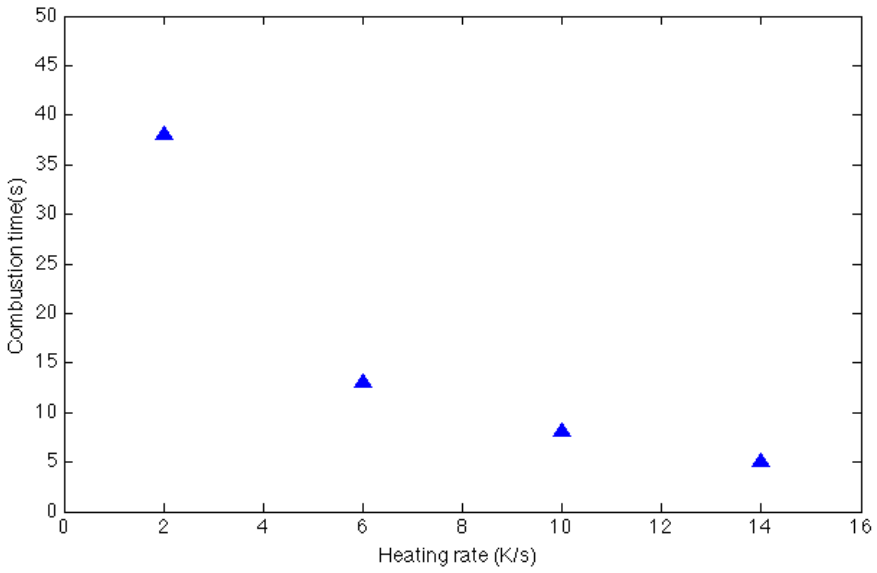

Fig.23.The Combustion time versus heating rate plot assuming 90% of the mass was burned in flaming combustion

As shown in Fig. 23, as the heating rate increases, the combustion time decreases. Since the amount of fuel being burned is the same for the four heating rates, Fig. 23 clearly indicates that combustion time is not an accurate indication of how much fuel was burned in the flaming combustion. Instead, the product of combustion time and heating rate was plotted against heating rate as shown in Fig.24.

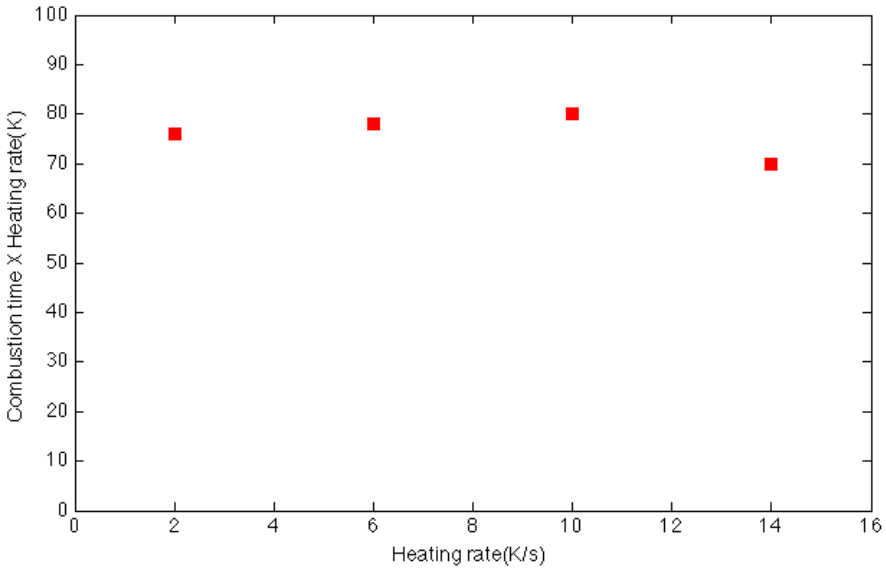

Fig.24.The product of combustion time and heating rate versus heating rate

As shown in Fig. 24, this value is nearly constant for all four heating rates, which indicates that this value can reflect the mass of fuel burned in flaming combustion more accurately than the combustion time. As shown in Fig. 25, the product of combustion time and heating rate was plotted in red squares as the criteria for determining the heating rate in FCC that could burn most of the fuel. Between 2-10 K/s this product increases with heating rate, suggesting that as the heating rate increases, more fuel mass is captured by the combustion process. From 10K/s on, the plateau is reached suggesting that no extra mass is captured by increasing the heating rate. However, if the heating rate goes too high, the combustion time would be sacrificed. Thus, taking all the factors into consideration, 10 K/s was chosen as the current heating of FCC.

It could be argued that at a heating rate of 10 K/s, the assumption that the sample was heated homogeneously and can be treated as thermally thin probably cannot be applied. However, the primary purposes of the FCC was to correlate to the cone calorimeter test data, thus, as long as the sample could burn almost completely and a solid connection between the small-scale FCC data and the bench scale cone calorimeter data could be acquired, whether the sample was thermally thin or not wouldn't affect the function of the FCC.

2.3.5. Sample heating rate and thermal feedback test

As the FCC was designed to separate the gas-phase combustion process from the condensed-phase combustion process, the heat feedback from the flame should be minimized as the energy from the pyro-probe should be the main energy source for the pyrolysis of the sample. Thus, several tests were done to seek the actual heating rate of the sample with and without the presence of a flame, and the impact of the flame on the sample heating rate was explored.

First, an experiment to test the actual heating rate of sample without the presence of a flame was designed. The experiment setup is shown in Fig. 25. A small ceramic tube with two holes was utilized to contain the thermocouple wires. The sample tube was stuffed with 30 mg of ceramic fibers with thermal conductivity and heat capacity similar to a polymer. The thermocouple bead was then inserted into the middle of the sample tube, buried in the ceramic fiber. Six tests were done in this configuration with the heating rate of the pyro-probe filament was at 10 K/s, as a normal FCC test. Then, additional 3 tests were done with the ceramic fiber removed; the thermocouple

bead was placed at the same location in an empty sample tube. Fig. 26 shows the test results.

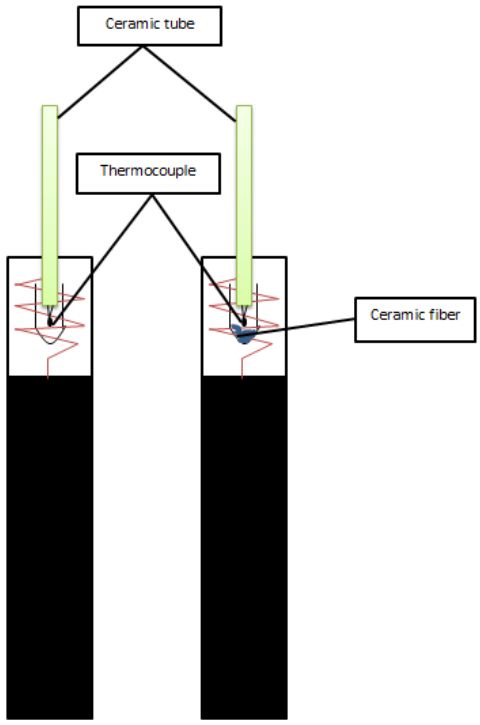

Fig.25.The experimental set-ups for measuring the heating rate of a sample without a flame with and without the presence of ceramic fiber in the sample tube

As Fig. 26 shows, the temperatures versus time profiles are highly repeatable. Between 60s and 140s, the temperature profile is almost linear with the heating rate of 6.8K/s. The presence of ceramic fiber in the sample tube did not change the heating rate profile indicates that one heating profile can fit various polymer sample burning conditions, since the thermal conductivity and heat capacity of air and ceramic fiber are very different from one another. This highly repeatable behavior of the sample heating rate would allow us to know the actual relationship between time and temperature in the sample and thus know the actual heating rate of the sample.

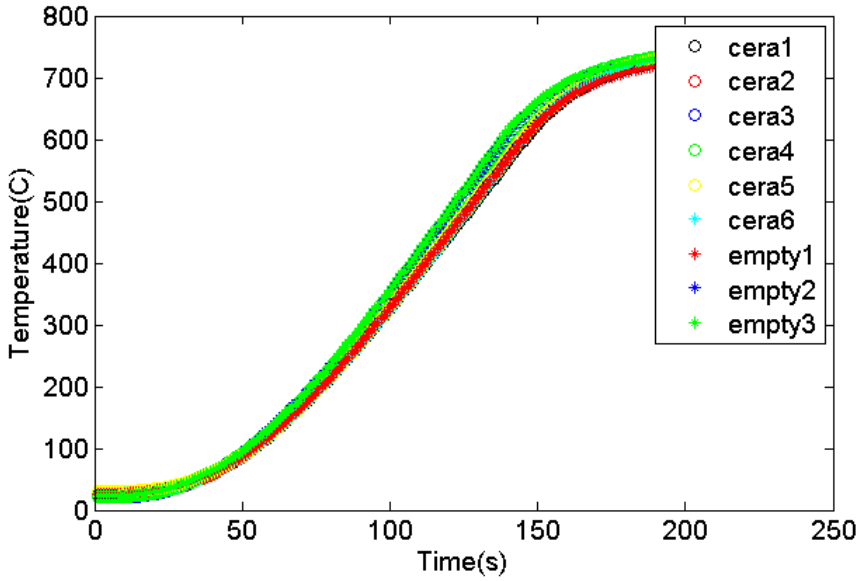

Fig.26. Results for the test of sample heating rate without a flame

Attempts to characterize the temperature profile in the sample tube while the flame was present proved unsuccessful. The configuration in Fig. 25 could not be utilized because heat would be conducted from the flame to the thermocouple bead. Thus, another setup shown in Fig. 27 was designed. The thermocouple bead was carefully inserted from the side of the pyro-probe into position in the sample tube. A small hole was punched on the wall of the quartz tube to allow thermocouple wires to pass through. Since the thermocouple wires were close to the pyro-probe coil, conduction from the heated coil to the thermocouple bead was present; it was not the biggest concern as the pyro-probe followed the same heating profile for all the tests, thus a baseline test without the presence of the flame can easily correct for the conduction error. It is the sealing problem of the hole in the quartz tube that resulted in failure to

produce accurate results. Since a high-temperature cement was not found at that time, the hole was left open. The test would fail when the pyro-probe filament reached approximately 700℃. The flame became extremely sooty and the thermocouple wire failed, leaving the inside of pyro-probe and the sample tube covered in soot.

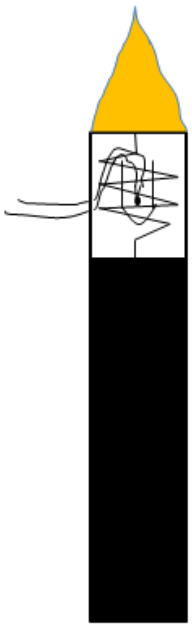

Fig.27.The experimental set-up for measuring the heat release rate of the sample with a flame

This might be explained by the observation that in diffusion flames, soot concentration could increase with the addition of oxygen to the fuel side of the flame. It was found that the oxygen addition to alkene fuel on the fuel side of the flame had a catalytic effect in triggering pyrolysis reactions in the fuel. [26] Since propane was used to generate the flame, it is possible that the entrainment of the air through the hole triggered the pyrolysis of propane and increased the soot formation in the process.

An alternative experiment was designed to observe the temperature profile in the sample tube with and without a flame present as the pyro-probe coil was cooling from approximately 600℃. The thermocouple configuration for this test was the same as in Fig. 27 with the hole in the quartz tube sealed with regular cement. The pyro-probe was heated and held at 800℃ with the thermocouple temperature plateauing at approximately 570℃, the purge gas was propane with the flow rate of 60sccm and ignited. The pyro-probe coil was deactivated, and thermocouple data was recorded. Another test without igniting the propane to create a flame as the pyro-probe cooling down was conducted with the other settings remaining the same; the purge gas was still propane at a flow rate of 60sccm. Fig. 28 shows the result.

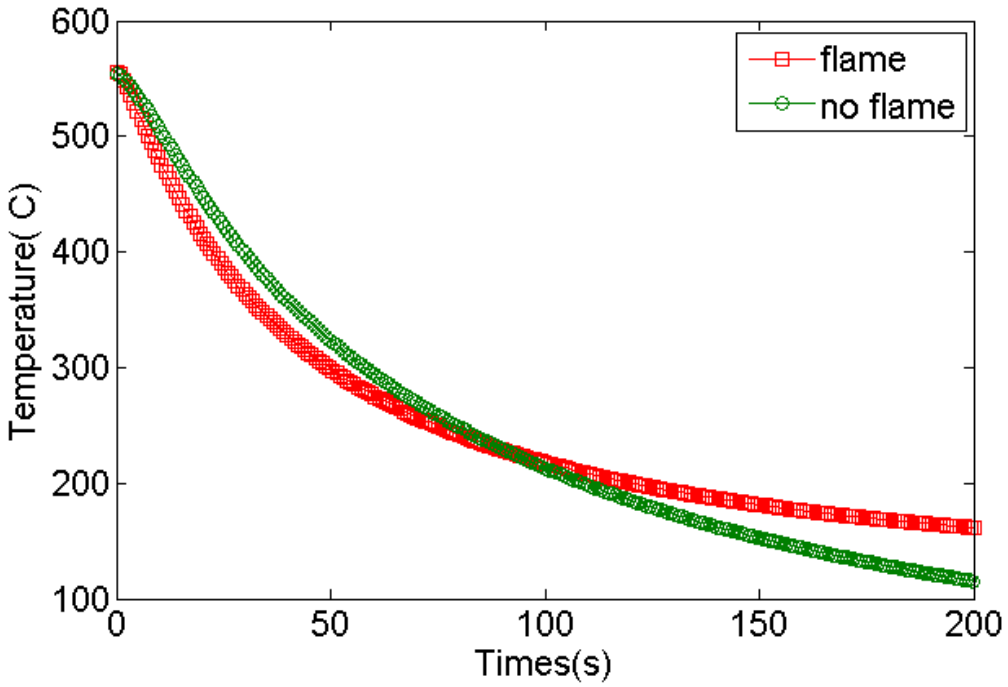

Fig.28.The temperature profile of the sample tube cooling down with and without a flame

The result showed that with a flame, the temperature in the sample tube dropped slightly faster in the beginning but slower after about 80 seconds. This slowing of the temperature drop as a flame presented was likely due to the flame heating up the quartz tube, causing the rate of heat loss to decrease. Although the result could not apply to the heating profile of a sample, it served as an indication that the impact of the flame on the sample heating was small.

2.4 Optimization of FCC

2.4.1 Reducing condensation test

After the heating rate of the pyro-probe filament was chosen, Polyethylene (PE) samples were tested because it was known that PE had a tendency to condense. A condensation problem was observed when pyrolyzing a 30mg PE sample at 10 K/s with the purge gas being N_2 with a flow rate of 10sccm. As the sample boiled vigorously, a large amount of the volatiles coming from the sample tube did not immediately enter the flame. It was observed that the volatiles recirculated inside the pyro-probe, forming small droplets on the inside wall of the quartz tube. The left picture on Fig. 29 shows the quartz tube after one experiment of PE in this configuration.

Condensation meant that there was unburned mass in the sample, the actual volatile mass engaged in flaming combustion was less than the initial mass of the sample minus the char yield, which lead to incorrect calculation of the combustion efficiency.

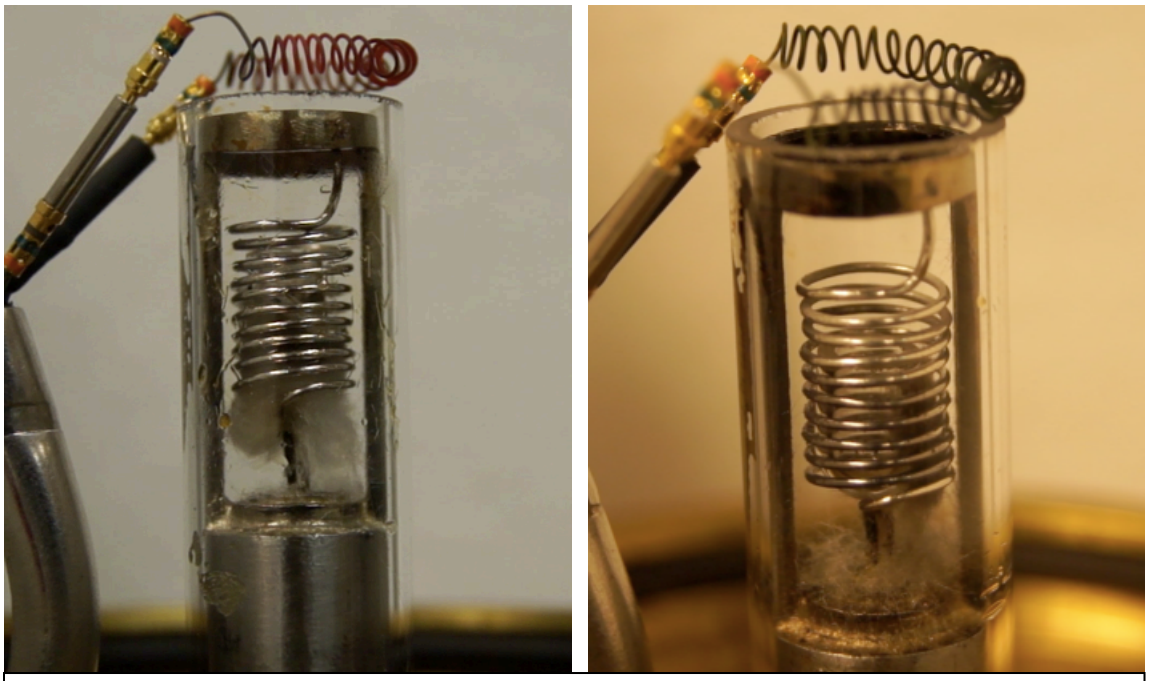

Fig. 29.Comparison of condensation between N_2 rates of 10sccm and 100sccm

The condensation happened when the pyrolyzed volatiles did not travel fast enough to the flame and the temperature of the inner wall of the quartz tube was relatively low so that the volatiles condensed upon touching the wall. Several approaches could be taken to address this problem:

1. Bring up the temperature of the quartz tube;
2. Increase the upward traveling speed of the pyrolysis products by increasing the purge gas flow rate;
3. Decrease the distance for the pyrolysis products to travel from the top of the sample tube to the flame.

The first method of warming up the quartz tube is difficult to approach and would change the heat transfer conditions and the heating rate of the sample. Thus, increasing the purge gas flow rate and decreasing the traveling distance for the pyrolysis products were the focuses chosen.

The N_2 flow rate in the purge gas line was first increased to 50sccm and 100sccm for burning PE. Two tests with sample mass of approximately 32mg were conducted at each heating rate. An N_2 flow rate of 100sccm was found to generate a consistent PE flame and keep the quartz tube clean as shown in the right picture of Fig.29. Increasing N_2 tests were also repeated on PMMA samples.

Increasing N_2 tests were also conducted for the two materials as the relative positions of the pyro-probe and the quartz tube were changed. As shown in Fig. 30, the pyro-probe was moved up from its original position where its top ring was located 2mm below the top opening of the quartz tube (referred to as probe-down position) to 2mm above the top opening of the quartz tube (referred to as probe-up position). Thus, the distance for the pyrolysis products to travel before engaging in combustion process was shortened. The combined effect of shortening traveling distance and increasing purge gas flow rate was shown in Fig. 31 for PE and Fig.32 for PMMA.

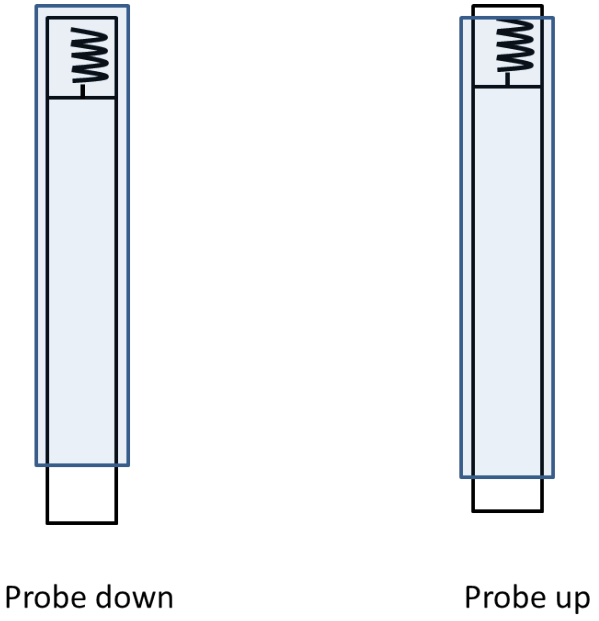

Fig.30.Change probe position set-up

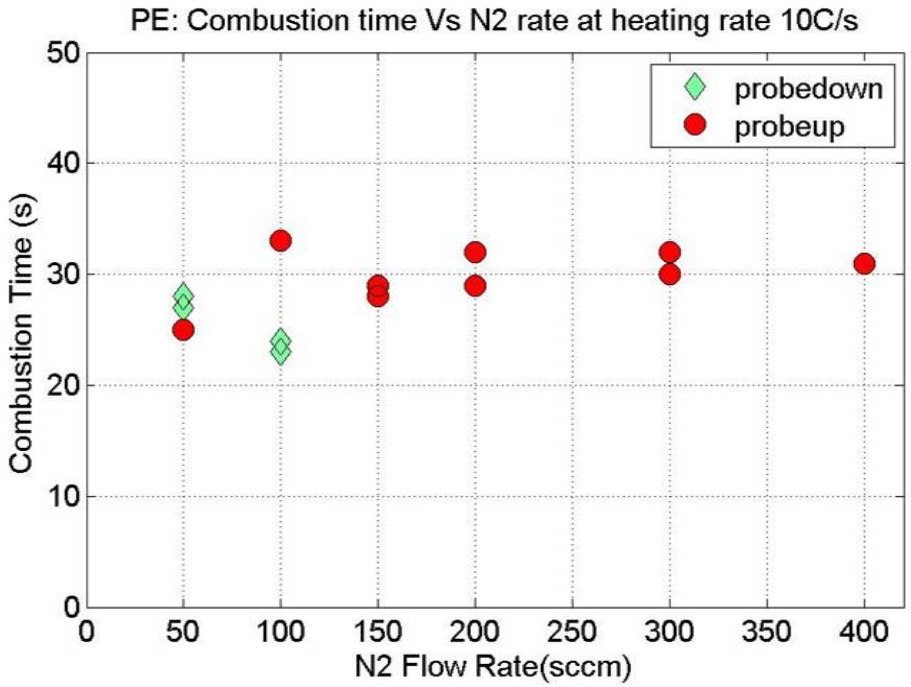

Fig.31.Combustion time versus N_2 flow rate test at probe-up and probe-down for PE

As shown in Fig.31, at the probe down configuration, the combustion time of decreased slightly as the N_2 flow rate increased from 50sccm to 100sccm, though the condensation was lighter at 100sccm. Changing to the probe-up configuration increased the combustion time of PE significantly.

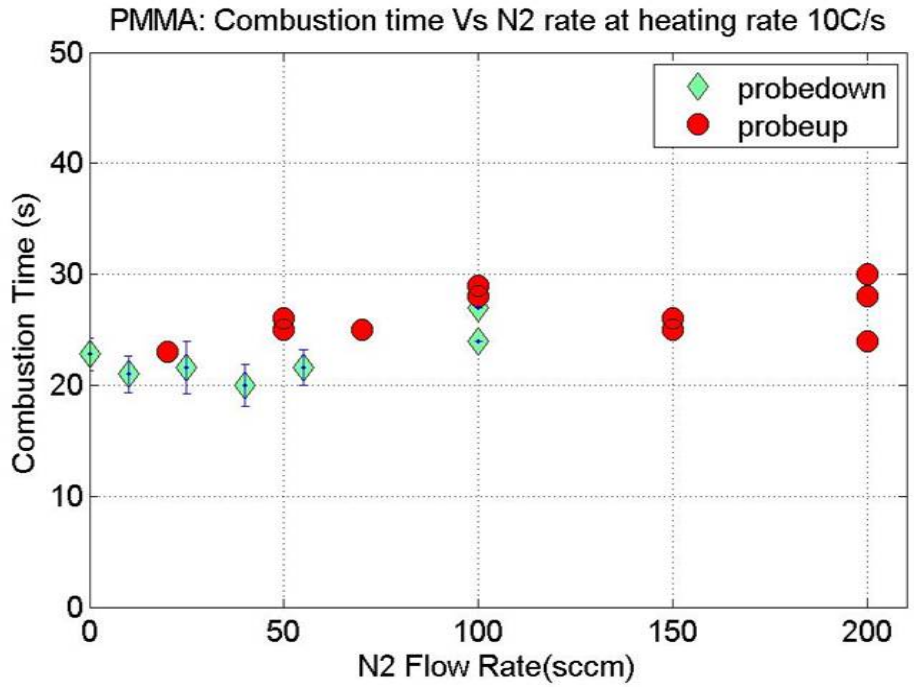

Fig.32. Combustion time versus N_2 flow rate test at probe-up and probe-down for PMMA

Fig. 32 shows the combustion time versus N_2 flow rate for PE at probe-up and probe-down configurations. Combined with Fig.31, it was obvious that compared with the probe-down configuration, the probe-up configuration generated higher combustion time overall for both PMMA and PE, which confirmed that the earlier proposed method of decreasing the travel distance of the pyrolysis products would work. At the probe-up configuration, the combustion time of both materials increased as the N_2 flow rate increased up to 100sccm. After 100sccm the combustion time did not change significantly and even went down slightly at 150sccm for PMMA. Although

the increase of N_2 could help reduce condensation, the introduction of N_2 would decrease the flame temperature, change the flame structure and dilute the fuel. Thus, as 100sccm was the lowest flow rate that could address the condensation problem and improve the combustion time, it was chosen to be the N_2 flow rate for PMMA and PE. Also, as PMMA was a typical oxygen containing polymer that does not tend to condense, but easy to dilute and PE was a typical polymer, condenses significantly, and 100sccm N_2 flow rate allowed both materials to achieve high combustion time, 100sccm was used as default purge gas flow rate for all the polymers testing in FCC from that point.

2.4.2 Sample tube and igniter test

The sample tube used in the prior experiments had an inner dimension of 4mm, an outer diameter of 6mm and 8mm length (further referred to as short sample tube) which had just the enough volume to hold 30mg of PMMA powder, thus a bigger sample tube was desired. The bigger sample tube (further referred to as long sample tube) had the inner diameter of 4mm, an outer diameter of 6mm the same as the old sample tube and a 14mm length. Since the location of the bottom of the sample tube did not change, the top opening of the long sample tube was closer to the top of the pyro-probe as shown in Fig. 33, thus the travel distance for the pyrolysis products was further shortened. The igniter was also changed from the prior large one to a smaller one as shown in Fig. 34 to minimize the heat load to the sample. The combined effect of elongating sample tube and reducing igniter coil length was shown in Fig. 35 for PMMA and Fig. 36 for PE.

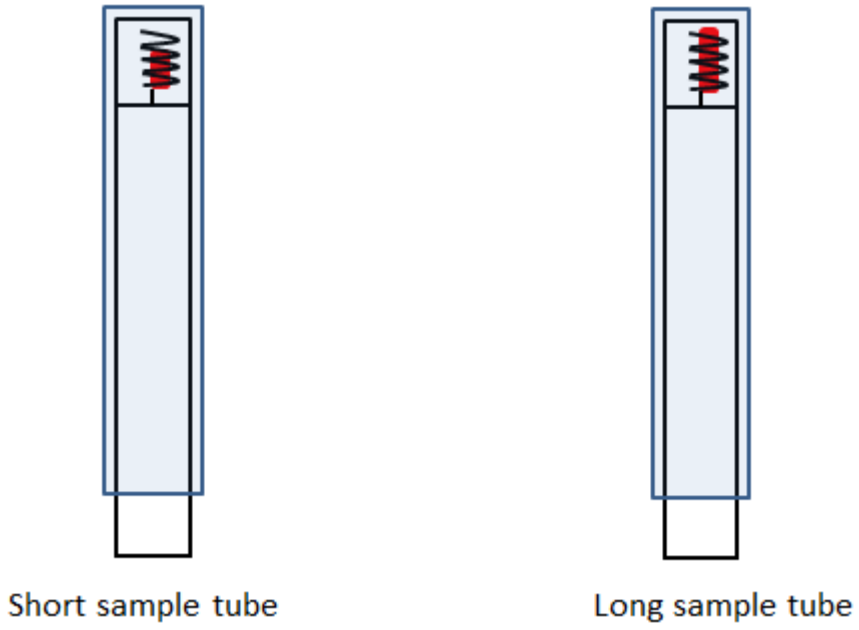

Fig.33.Short sample tube versus long sample tube

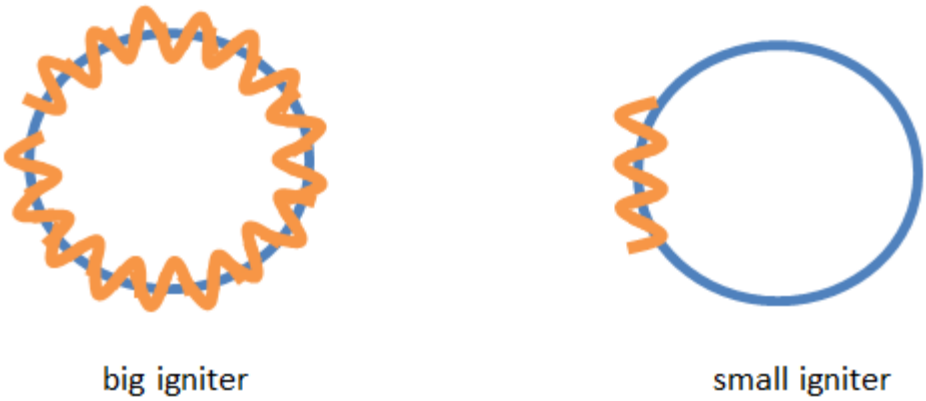

Fig.34.Big igniter versus small igniter

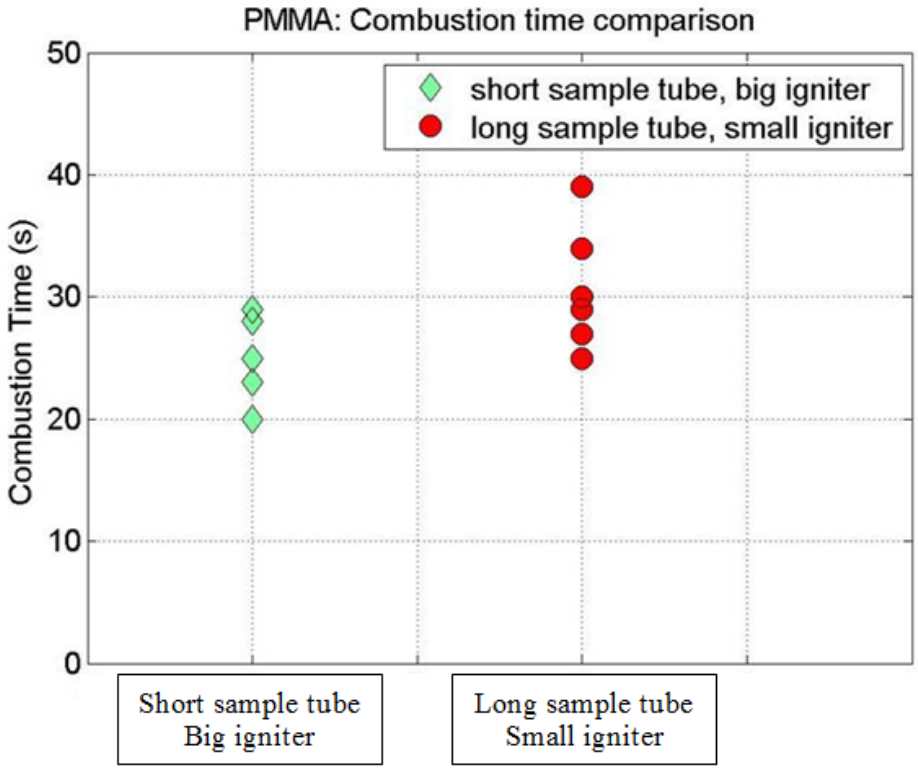

Fig.35.Changing sample tube and igniter result for PMMA

(Heating rate: 10K/s, purge gas N_2: 100sccm)

The sample masses in long sample tubes were kept the same as the previous tests, which is 30mg. The long sample tube and small igniter configuration provided an on-average higher combustion time for PMMA as shown in Fig. 35. Fig. 36 shows the result for PE. Three tests were performed at each configuration: all three data points overlapped for the big igniter and short sample tube configuration, two data points overlapped at the small igniter and big sample tube configuration. The tests demonstrated repeatability. For PE, the long sample tube and small igniter configuration also generated higher combustion times.

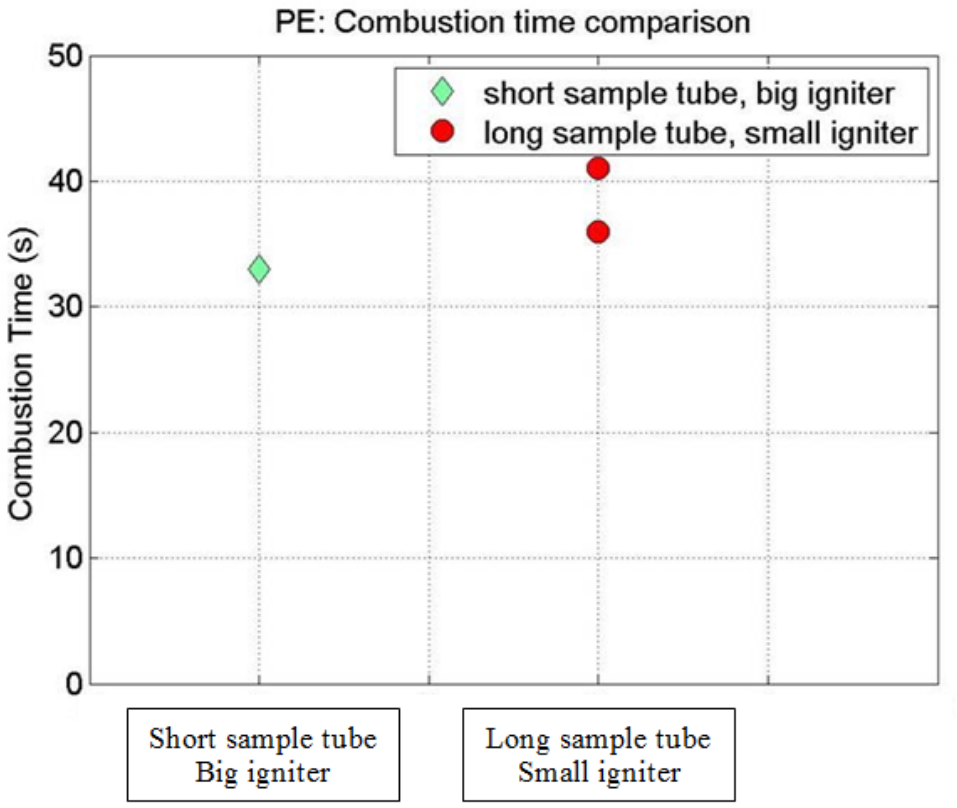

Fig.36.Changing sample tube and igniter result for PE

(Heating rate: 10K/s, purge gas N_2: 100sccm)

2.4.3 Pyro-probe sample holder re-design

By shifting pyro-probe above the quartz tube, the condensation problem was relieved and the combustion time increased. However, at this configuration as shown in the left picture in Fig. 37, the flame would sit on the pyro-probe, which was made of metal that was potentially acting as a heat-sink. To prevent this from potentially altering the combustion conditions and cooling the flame, a new pyro-probe modified by the CDS Analytical Company was utilized with the filament location changed

while keeping the relative coil location the same as the prior probe-up configuration as shown in the right part of Fig. 37.

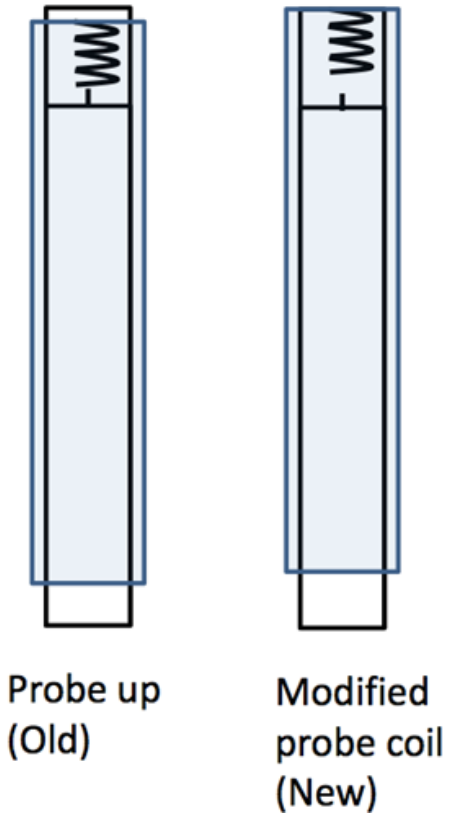

Fig.37.Old probe-up versus modified pyro-probe

Five tests were performed on the modified pyro-probe configuration for both PMMA and PE. The combustion time was recorded and compared with the old pyro-probe up setting. The comparison of results for PMMA is plotted in Fig. 38 and PE in Fig. 39. As Fig. 38 and Fig. 39 show, by using the modified pyro-probe with the probe-down configuration, the combustion time increased slightly.

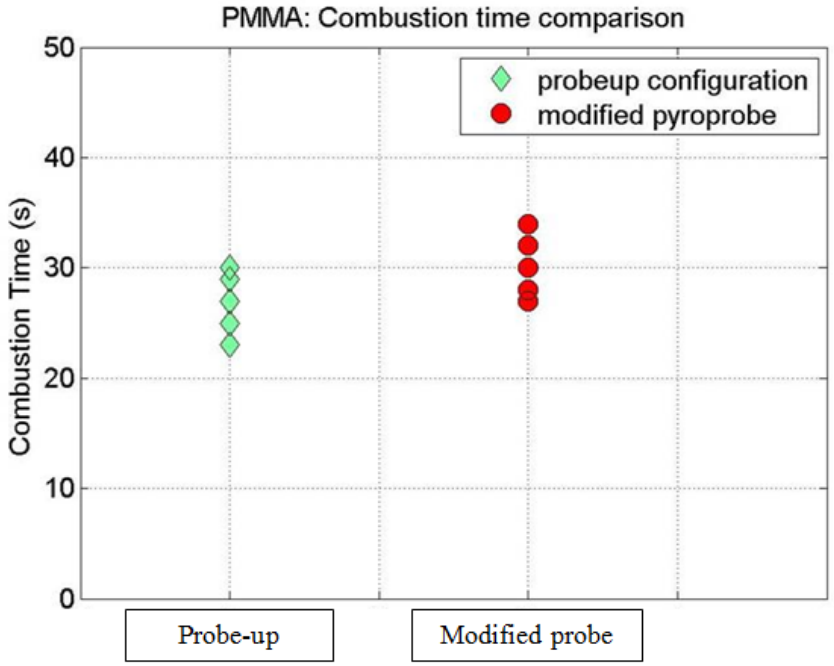

Fig.38.Combustion time comparison between probe-up and modified probe configuration for PMMA (Heating rate: 10K/s, purge gas N_2: 100sccm)

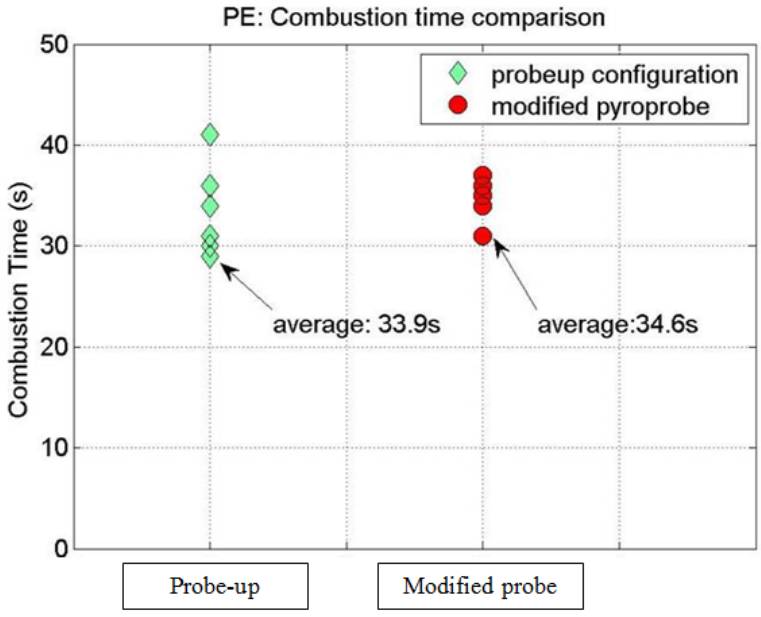

Fig.39.Combustion time comparison between probe-up and modified probe configuration for PE (Heating rate: 10K/s, purge gas N_2: 100sccm)

2.5 FCC repeatability and accuracy test

To characterize the repeatability and accuracy of the FCC, PMMA tests were conducted in the FCC and heat release curves were obtained. PMMA was chosen to be the test material because it is known to burn relatively cleanly with litter soot and char, therefore it tends to burn to completion, making it an ideal reference case. To test the accuracy of the FCC, it is reasonable to compare the measured total heat release (THR) to the literature value for PMMA that is $25.1 kJ/g$. [27]

5 PMMA powder samples with the approximate mass of 30mg were tested in the FCC. THR normalized by initial weight was calculated by two methods. The first method introduced in section 1.4.1 obtained the THR via Equation 9 and the average value was $24.61 \mp 0.29 kJ/g$. The second method introduced in 1.4.1 obtained the THR via Equations 10 and the average value was $23.66 \mp 0.23 kJ/g$. The first method generated the THR values on average closer to the literature value of PMMA, suggesting that the first method was more accurate. The average heat release rates versus time curves calculated using method 2 for the 5 tests are shown in Fig.40 with the uncertainty being two standard deviation divided by the square root of test number. The average percentage error of the instantaneous heat release rate for the five tests was 9.25%. This result showed that the FCC was accurate and provided repeatable results.

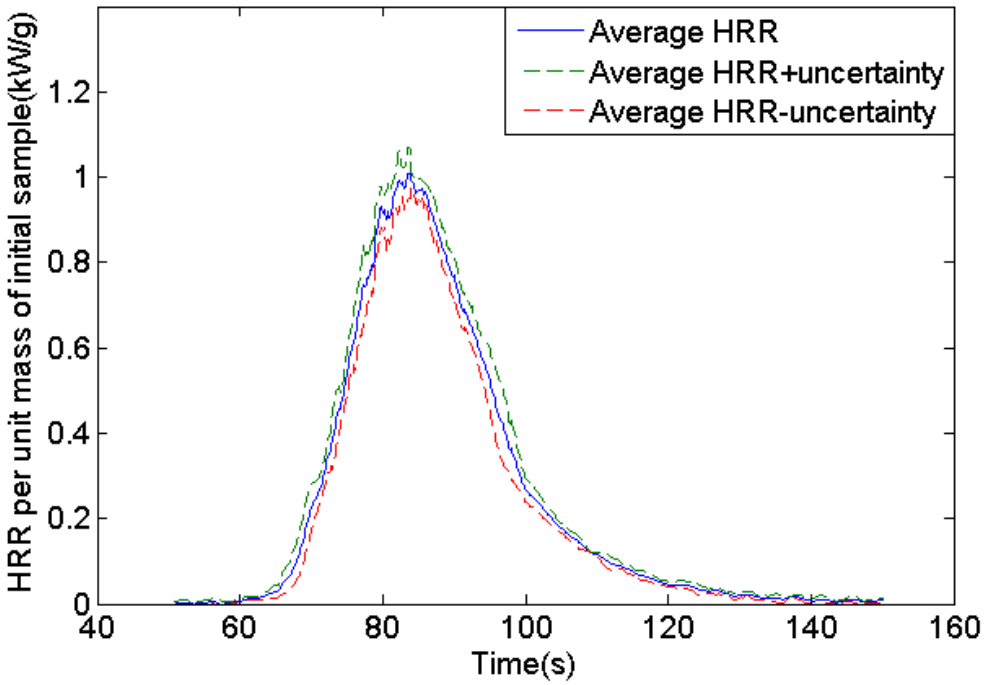

Fig.40.The average heat release rate curve of FCC for 5 PMMA tests

Chapter 3: Case study

3.1 Sample Material

Standard Cone Calorimeter tests, Standard Microscale Combustion Calorimeter tests and Flaming Combustion Calorimeter tests were performed on the followings three materials: BASF polystyrene 158K, and a well-blended product of 90% BASF polystyrene 158K and 10% Saytex HP3010 flame retardant, and a well-blended product of 60% BASF polystyrene 158K and 40% Saytex HP 3010 flame retardant. Saytex HP 3010 flame-retardant is a highly effective brominated polystyrene product with 68.5% of bromine by weight. [28] The chemical structure of Saytex HP 3010 is shown in Fig.41. In this paper, for simplicity reasons, BASF polystyrene 158K will be called PS, BASF polystyrene 158K with 10% flame retardant will be called PS-FR1 and BASF polystyrene 158K with 40% flame retardant will be called PS-FR2. Table 1 illustrates the name of the material, the actual composition and the actual weight percentage of bromine.

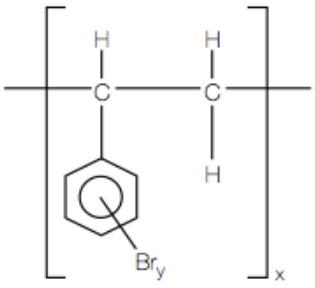

where x is proprietary and y is approximately 2.7

Fig. 41.The chemical formula of Saytex 3010 flame retardant

Table.1. Sample materials

Material name in this paper	Actual composition	Weight percentage of Bromine (%)
PS	BASF polystyrene 158K	0
PS-FR1	BASF polystyrene 158K 90%+ Saytex HP 3010 10%	6.85
PS-FR2	BASF polystyrene 158K 60%+ Saytex HP 3010 40%	27.4

3.2 Cone Calorimeter (CC) Experiments

The samples used in the cone calorimeter tests had sizes of 100mm×100mm, and thicknesses of 6.35mm. Prior to testing, the samples were conditioned in an environment of 30% relative humidity for at least 48hours. By conditioning the sample, a better reproducibility of the tests output could be expected.

After weighing the specimen, a piece of aluminum foil with the thickness of 0.025mm was used to wrap the specimen. With the more reflective side of the aluminum foil facing towards the specimen, the foil was cut so that the back and the sides of the specimen can be held tightly within. The four sides of the foil were raised 2mm higher than the specimen edges in order to contain the material while the specimen was melting and pyrolyzing during the test. The aluminum foil serves to minimize any mass transfer at the specimen edges that may occur as well as keeping the material from dripping onto the refractory blankets that lie beneath the specimen. For the PS-FR2 specimens, two layers of aluminum foil were used to cover the back

of the specimen, because it is observed that one layer of aluminum foil was partly disappeared after the test, probably reacted with HBR, as shown in Fig.42.

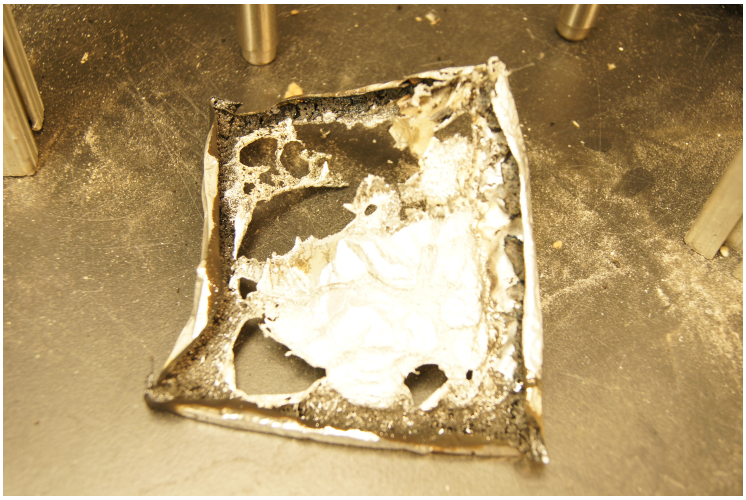

Fig.42.One layer of aluminum foil burned out after one PS-FR2 test

The prepared specimen was then placed on the sample holder, on top of 13mm refractory ceramic fiber blanket of 100mm × 100mm. The cone calorimeter tests were carried out according to ASTM E 1354 [29] standard. The heat flux was set to be 50kW/m^2 and the exhaust flow rate was 0.24m^3/s. The samples were very sooty; the soot filters needed to be changed each time after each test and the sampling ring needed to be cleaned daily.

3.3 Micro-scale Calorimeter Experiments

Powdered samples were used for the MCC test. Bottles containing the polymer powders were conditioned in a conditioning box with a relative humidity of 30% for at least 48 hours before the test. A Microbalance that can measure up to 0.001mg was used to weigh the sample mass. A small ceramic pan was used to contain the sample. The weight of the empty pans, pans contain samples (the sample mass was

approximately 2.5- 3mg) and pans after test were weighed. Test procedures follow the standard operation of the MCC. [30]

3.4 Flaming Combustion Calorimeter Experiments

The samples used in the FCC tests were the same as those used in the MCC tests. The bottle containing the polymer powders were conditioned in a conditioning box with a relative humidity of 30% for at least 48 hours before the test. A microbalance with the uncertainty of $\pm$ 0.001mg was used to weigh the sample. The weight of the empty quartz tube, the quartz tube containing sample with the mass of approximately 30mg and the quartz tube after the test were weighed for each test. The soot filter was also weighed before and after each test so that the soot yield could be determine.

Prior to the test, the co-gas flow meter was set to 4 slpm and the purge gas flow meter was set to 100sccm. The pyro-probe was programed to hold at 30℃ for 5s, then follow the heating rate of 10 K/s until it reached the final temperature of 1200℃ and then to remain at 1200℃ for 2 min. The programming software of CDS 5000 pyroprobe is shown in Fig. 43. A Labview program was developed to monitor and acquire the flow meter flow rate and O_2 concentration signals. When the flow rate signal and O_2 concentration signal were steady, the igniter was turned on and the pyro-probe was started. The data acquisition program began at the same time when the pyro-probe went to the "ramp" step, i.e. the step where the temperature climbed at the heating rate of 10K/s. As soon as a steady flame formed, the igniter was

deactivated. The data acquisition program would run for 200 seconds before shut off automatically.

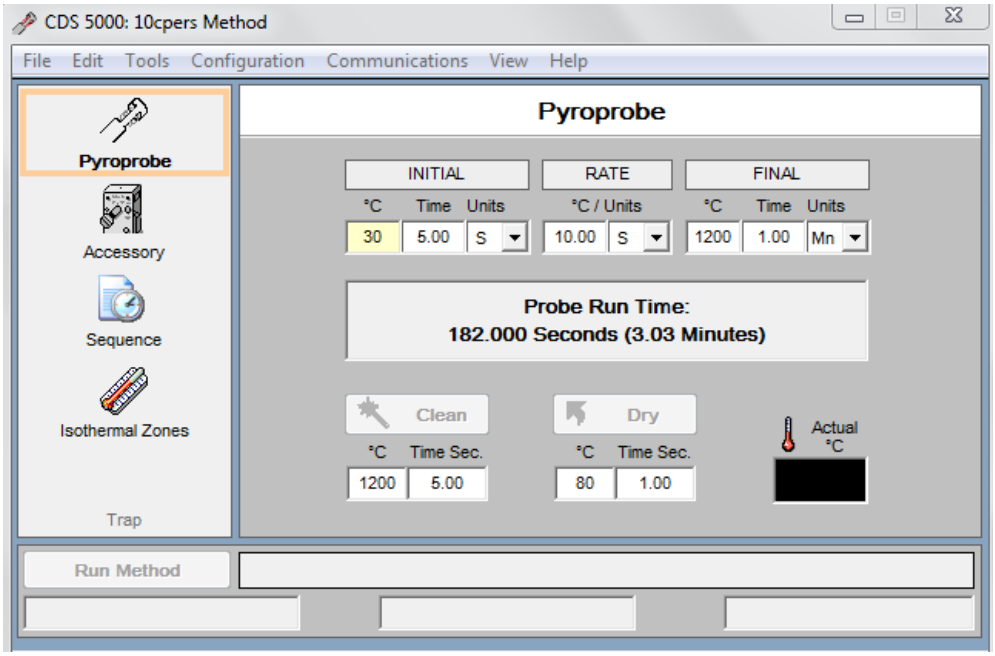

Fig.43.The CDS 5000 pyro-probe programming software

3.5 Test matrix

The test matrix for the case study of PS, PS-FR1 and PS-FR2 performed on the CC, MCC and FCC is shown in Table.2.

Table.2.The test matrix for the case study

	Sample	Tests per sample	Sample mass	Heating condition	Flow condition
CC	PS PS-FR1 PS-FR2	3	43-55g	Constant heat flux: 50 Kw/m^2	Exhaust flow rate: $0.24m^3/s$
MCC	PS PS-FR1 PS-FR2	5	2-3mg	Constant heating rate: 1K/s	O_2:20sccm N_2:80sccm
FCC	PS PS-FR1 PS-FR2	3	29-31mg	Constant heating rate: 10K/s	Air: 4slpm Purge gas N_2: 100sccm

Chapter 4: Result and Discussion

4.1 Test Results

All experimental methods used in this study were based on the oxygen consumption technique introduced in section 1.4.1. The result of the CC, MCC and FCC tests are summarized in table 3 and 4.

Table 3.Summary of cone calorimeter data obtained at the external heat flux of 50 kW/m^2

Material	Avg. HRR kW m^{-2}	THR kJ g^{-1}	Avg. MLR g m^{-2} s^{-1}	Char wt.%
PS	832.80±3.70%	28.80±0.45	35.70±1.47	0.00
PS+10 wt.% PS-Br (6.85 wt.% Br)	685.70±4.60%	21.20±0.78	38.90±0.29	0.00
PS+40 wt.% PS-Br (27.4 wt.% Br)	345.00±12.20 %	8.80±0.63	42.04±4.35	1.30±0.39

The THR value was divided by the initial weight of the sample. The average heat release rate (Avg. HRR) and the average mass loss rate (Avg. MLR) were obtained from the data collected during the time between the initial increase of the heat release rate above 150 kW m^{-2} and its final decrease below 150 kW m^{-2}.

Table.4. Summary of MCC and FCC data

Material	MCC THR kJ g^{-1}	MCC Char wt. %	FCC THR 1 kJ g^{-1}	FCC THR2 kJ g^{-1}	FCC Char wt.%	FCC Soot wt. %
PS	38.10±0.65	0.26±0.56	34.60±0.34	32.04±0.19	0.01±0.01	17.80±0.80
PS+10 wt.% PS-Br (6.85 wt.% Br)	35.20±0.48	0.46±0.43	29.86±0.64	28.28±0.20	0.02±0.02	20.90±0.45
PS+40 wt.% PS-Br (27.4 wt.% Br)	22.70±0.27	2.80±1.30	16.92±0.26	16.31±0.45	0.32±0.09	26.00±1.60

Where FCC Char wt. % = mass of char/ initial sample mass, FCC Soot wt. %= mass of soot/initial sample mass. The THR value was divided by the initial weight of the sample. The FCC THR was calculated by two methods. The first method was calculated using Equation 9 and the second method was calculated using Equation 10. The MCC THR was calculated using Equation 10.

4.2 Analysis and Discussion

To analyze the THR and Avg. HRR trends, it was necessary to determine the heats of complete combustion (ΔH_C) of the material under study. Since the atomic composition of pure PS and the Saytex HP 3010 flame retardant were known, and the ratio of pure PS to Saytex HP 3010 flame retardant in PS-FR1 and PS-FR2 were known, the atomic composition of PS-FR1 and PS-FR2 could be determined. Then, the heats of complete combustion could be calculated from the stoichiometry of the

corresponding reactions and the heat release constant (13.1 kJ g^{-1}). A stoichiometric complete combustion reaction is shown in equation 14:

$$C_xH_yO_zBr_k[gas] + \left(x + \frac{y-k}{4} - \frac{z}{2}\right)O_2 = xCO_2 + \frac{y-k}{2}H_2O[gas] + kHBr \qquad [14]$$

The chemical formula of PS was $(C_8H_8)_n$, the chemical formula of Saytex HP 3010 flame retardant was $(C_8H_{5.3}Br_{2.7})_n$. PS-FR1 was made up of 10% of Saytex flame retardant of 90% of PS by weight. By translating mass fraction to mole fraction, that PS-FR1 was made up of approximately 96% of PS and 4% of Saytex flame retardant by mole could be calculated, thus the chemical formula of PS-FR1 was calculated to be $C_8H_{7.892}Br_{0.108}$. The chemical formula of PS-FR2, calculated through the same approach, was $C_8H_{7.514}Br_{0.486}$. The heats of complete combustion (ΔH_C) of the material used in this study were calculated via Equation 15[17] and are shown in table 5.

$$\Delta H_C = 13.1 * \Delta m_{O_2} \qquad [15]$$

Table.5. Heats of complete combustion of materials and carbon normalized by weight

Material	PS	PS+10 wt.% PS-Br (6.85 wt.% Br)	PS+40 wt.% PS-Br (27.4 wt.% Br)	Carbon
ΔH_C (kJ g^{-1})	40.3	37.42	28.75	34.9

Knowledge of the heats of combustion makes it possible to determine the gas-phase combustion efficiency in CC, MCC and FCC by using Equation 16. Note that the char is assumed to consist of pure carbon.

$$Comb.Eff. = \frac{THR}{\Delta H_C(material) - \Delta H_C(char) * ch.yld.} \quad [16]$$

Where ch.yld. = mass of char/ initial sample mass. The combustion efficiencies for PS, PS-FR1 and PS-FR2 in CC, MCC and FCC were plotted in Fig.44.

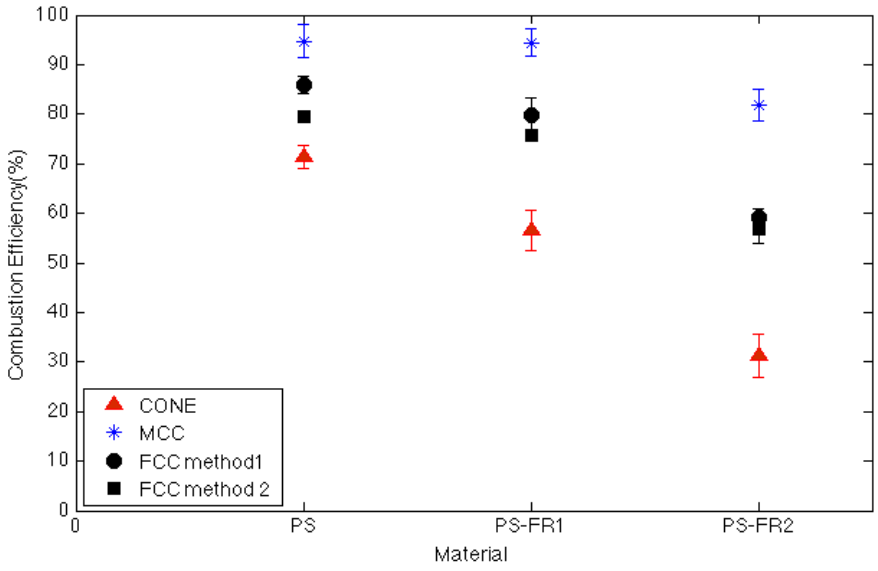

Fig.44. Gas-phase combustion efficiencies for the three test materials

As shown in Fig. 42, the CC and FCC dependencies were consistent with the notion that bromine acted as a suppressant of the gas-phase combustion. For the MCC, the difference in gas-phase combustion for pure PS and PS-FR1 (6.86 wt. % of bromine) was indistinguishable. The gas-phase combustion for PS-FR2 (27.4 wt. % of bromine) dropped to 81% in MCC. The FAA report on the heats of combustion of brominated epoxies showed that the addition of brominated compounds produces a slight increase in gas-phase combustion efficiency for MCC. [21] Similar results have

also been reported from other labs using the MCC. [21] One explanation for this drop was that PS-FR2 samples didn't reach complete combustion in the MCC. However, the MCC in our lab detected the gas-phase combustion efficiency drop for PS-FR2 material.

The FCC was definitely detecting the gas phase combustion inhibition effect of bromine, the gas phase combustion efficiency calculated in FCC was sensible to even the slight increase of bromine of 6.85%. The FCC however, did not capture the effect to the same extent as the cone calorimeter. The difference in flame sizes in the FCC and CC could be a possible explanation to this result.

The method 1 was considered more accurate than method 2 since the inlet flow rate was monitored by the mass flow controllers and it was observed that during the test, the inlet flow rate remained essentially unperturbed. Plus, as stated in section 2.4.5, method 1 generated an average THR value closer to the literature value of PMMA than that generated by method 2. Thus, the following analysis uses the method 1 calculation for THR.

Since in FCC, soot yield was measured. Thus, the theoretical maximum combustion efficiency in the FCC can be calculated assuming that soot is the only product of incomplete combustion through Equation 17:

$$CE_{theory} = \frac{THR - \Delta H_c(soot) * soot.yld - \Delta H_c(char) * char.yld}{\Delta H_C - \Delta H_C(char) * char.yld} \qquad [17]$$

Where, soot.yld= mass of soot/initial sample mass.

By plotting the theoretical combustion efficiency with the experimental combustion efficiency, the contribution of soot in the gas phase combustion efficiency drop could be accounted for. The plot is shown in Fig.45.

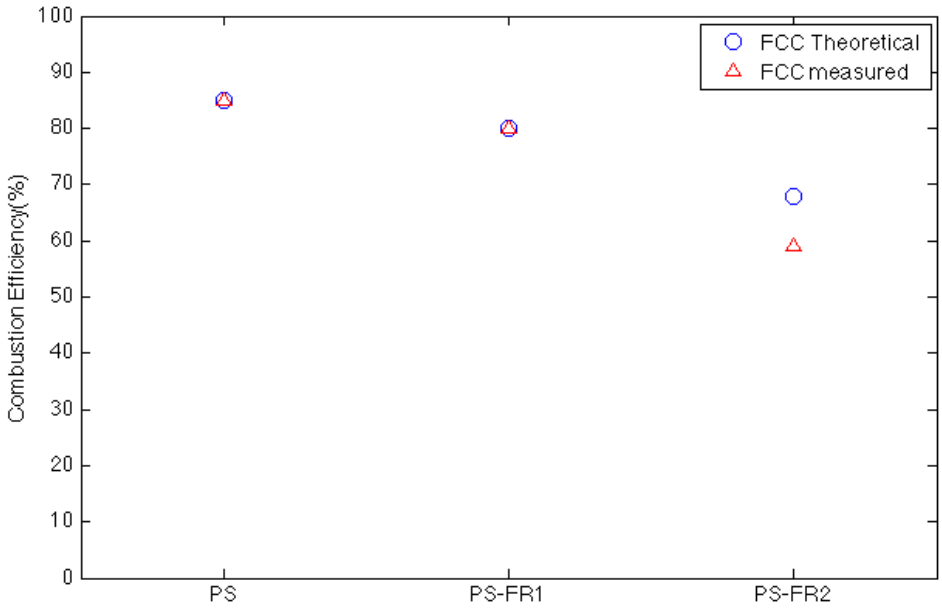

Fig.45.The comparison of combustion efficiencies between the theoretical and experimental data

Fig. 45 shows that for PS and PS-FR1, the formation of soot alone accounted for the combustion efficiency drop. For PS-FR2, the combustion efficiency drop was mainly caused by soot, but the production of CO and other incomplete combustion products also took place.

Assuming that the only incomplete combustion products occurred in the combustion of PS-FR2 are carbon and carbon monoxide, the combustion reaction for PS-FR2 can be written in the following form.

$$C_xH_yBr_k + aO_2 \rightarrow bCO + dCO_2 + eC + \frac{y-k}{2}H_2O + kHBr \quad [18]$$

With x equal to 8, y equal to 7.514, k equal to 0.486.

Assuming that the char and soot contain pure carbon, we have,

$$\frac{(char.yld + soot.yld) * Mass_{sample}}{MW_{carbon}} = \frac{Mass_{sample}}{MW_{sample}}e \quad [19]$$

Thus,

$$e = \frac{(char.yld + soot.yld) * MW_{sample}}{MW_{carbon}} \quad [20]$$

Consider the conservation of C atom,

$$x = b + d + e \quad [21]$$

Consider the conservation of O atom,

$$2a = b + 2d + \frac{y-k}{2} \quad [22]$$

Since the THR is calculated by 13.1kJ/g-O_2 multiplies the mass of the oxygen consumed, a can be calculated from the following equation,

$$\frac{THR * Mass_{sample}}{13.1 * MW_{O_2}} = \frac{Mass_{sample}}{MW_{sample}}a \quad [23]$$

Thus,

$$a = \frac{THR * MW_{sample}}{13.1 * MW_{O_2}} \quad [24]$$

Thus, with two equations (21, 22) and two unknowns (b, d), b and d can be solved. The CO yield can thus be calculated through the following equation,

$$CO.yld = \frac{b * MW_{CO}}{MW_{sample}} \times 100\% \quad [25]$$

The CO yield for PS-FR2 was then calculated to be 39.4%. The CO yield was 0 for PS and PS-FR1.

Chapter 5: Conclusion

In this study, a new instrument called the Flaming Combustion Calorimeter was designed and implemented to measure the heat release rate of flaming combustion of milligram scale polymers through oxygen consumption technique and detect the gas phase combustion inhibition effect by brominated flame retardants.

The oxygen consumption technique principle was studied and the embodiments of the principle: the cone calorimeter and the micro-scale combustion calorimeter were studied and a micro-scale combustion calorimeter was built and put in to operation by me and another colleague (Fernando Raffan). The possible assumptions for the inlet flow rate and inlet oxygen consumption in the implementation of oxygen consumption technique was discussed in detail and two methods were used in the FCC to calculate the heat release rate.

Several preliminary tests and optimization tests were performed on FCC to determine the optimal setup for the test as well as important test parameters. In the optimum setup, a platinum coil with the heating rate of the coil being 10K/s heated the sample polymer, purge gas with a flow rate of 100sccm transported the pyrolysis products up to meet the air and igniter, and a laminar diffusion flame was ignited in well-ventilated flow conditions. The heat release rate was measured by using oxygen consumption technique. The soot yield and the char yield were measured.

The FCC results were very repeatable with the percentage error of the total heat released of 5 PMMA powder tests being 1.18% using method 1 and 0.97% using method 2. (Method1 and method 2 are two methods of calculating THR performed on the FCC test data introduced in section 1.4.1) The FCC was also sensitive to the addition of bromine to the test sample and was able to detect the decrease in gas phase combustion efficiency with the increase of bromine. The yield of carbon monoxide can also be calculated assuming that the char and soot produced in FCC consist of pure carbon. However, the FCC was not capturing the effect that bromine acts as gas phase combustion inhibitor to the extent that cone calorimeter was capturing.

The future work of this study includes increasing the flame size within the capability of the equipment to further correlate with cone calorimeter results, decreasing the purge gas nitrogen flow rate so that the flame structure would be less disturbed and modifying the instrument to be more user-friendly.

References

1. Shui-Yu Lu, Ian Hamerton, Recent developments in the chemistry of halogen-free flame retardant polymers. Prog. Polym. Sci. 27(2002) 1661-1712.
2. A. Dasari, Z. Yu, G. Cai, Recent Developments in the fire retardancy of polymeric materials. <doi>http://dx.doi.org/10.1016/j.progpolymsci.2013.06.006</doi>
3. Price D, Anthony G, Carty P. Introduction: polymer combustion, condensed phase pyrolysis and smoke formation. Fire retardant materials. Boca Raton FL: CRC Press LLC, 2001. P 1-30.
4. Bourbigot S, Duquesne S. Fire retardant polymers: recent developments and opportunities. J Mater Chem 2007; 17: 2283-300.
5. D. Indritz, J. Boris, E. Oran, Calculation of Physical Effects of Diluents on Flames. Paper presented at the 178th National American Chemical Society Meeting, Washington, DC, September 1979.
6. Dixon- Lewis, G., Twenty-Third Symposium(International) on Combustion, The Combustion Institute, Pittsburg, 1990, p.305-324.
7. R. Sonnier, B. Otazaghine, L. Ferry, Study of the combustion efficiency of polymers using a pyrolysis- combustion flow calorimeter.
8. Warnatz, J., Eighteenth Symposium (International) on Combustion, The Combustion Institute, Pittsburgh, 1981, pp.369-384.
9. V.Babushok, W. Tsang, Combust. Flame 123(2000) 488-506.
10. M. Alaee, RJ. Wenning, The significance of brominated flame retardants in the environment: current understanding, issues and challenges. Chemosphere 46(5):579-582.
11. R. Sheinson, J. Penner-Hahn, D. Indritz, Fire safety Journal 15(1989) 437-450; L.Brinbaum, D. Staskal, Brominated flame retardants: cause for concern? Environ Health Perspect. 2004 January; 112(1):9-17.
12. T. Yamada, M. Sagara, T. Kobayashi, flammability test for flame retardant plastic pallet. Fifteenth meeting of the UJNR panel of fire research and safety, March 1-7, 2000, Volume 1: 89-96.
13. S. –Y. Lu, I. Hamerton, Prog. Polym. Sci. 27 (2002) 1661-1712.
14. C.P. Fenimore, F.J. Martin, Mod. Plast. 44 (1966) 141.
15. G. Camino, L. Costa, E.Casorati, G.Bertelli, R.Locatelli, J. Appl. Polym. Sci. 35(1988) 1863.
16. Thornton, W.M. “The Relation of Oxygen to the Heat of Combustion of Organic Compounds.” Philosophical Magazine and Journal of Science, Series 6, (1917) 33:194, 196-203.
17. C. Hugget, Fire Mater. 4(1980) 61.
18. R. Lyon, R. Walters, S. Stoliarov, Principle and Practice of Microscale Combustion Calorimetry, FAA technical note, DOT/FAA/TC-12/53.
19. R. Lyon, R. Walters, Pyrolysis Combustion Flow Calorimetry, J.Anal.Appl.Pyrolysis 71(2004)27-46.

20. W.J. Parker, Calculations of the Heat Release Rate by Oxygen Consumption for Various Applications, NBSIR 81-2427-1.
21. S. Stoliarov, R. Walters, R. Lyon, Heats of Combustion of Brominated Epoxies, FAA technical note, DOT/FAA/AR-TN05/45.
22. R. Sonnier, B.Otazaghine, etc. Study of the Combustion Efficiency of Polymers Using a Pyrolysis-Combustion Flow Calorimeter, Comb. Flames (2013) http://dx.doi.org/10.1016/j.combustflame.2013.04.009.
23. A. Mouritz, A. Gibson, Fire Properties of Polymer Composite Materials, eISBN: 9786610745104.
24. Thornton, W.M. "The Relation of Oxygen to the Heat of Combustion of Organic Compounds." Philosophical Magazine and Journal of Science, Series 6, (1917) 33:194, 196-203.
25. www.cdsanalitical.com/instruments/pyrolysis/pyroprobe_5000.html
26. H.S.Hura, I. Glassman, Soot Formation in Diffusion Flames of Fuel/Oxygen Mixtures, 27th Symposium on Combusion, 1988/pp 371-378.
27. Richard E. Lyon, Advanced Fire Safety Materials For Aircraft Interiors, Thirteenth Meeting of the UJNR Panel on Fire Research and Safety, March 13-20, 1996, volume 2, pp 249-259.
28. Saytex HP-3010 Flame retardant description, Albemarle Corporation.
29. ASTM E 1354-13, Standard Test Method for Heat and Visible Smoke Release Rate for Materials and Products using an Oxygen Consumption Calorimeter.
30. ASTM D 7309-11, Standard Test Method for Determining Flammability Characteristics of Plastics and Other Solid Materials Using Microscale Combustion Calorimetry.